



Rapid Quenching of Galaxies at Cosmic Noon

Minjung Park¹, Sirio Belli², Charlie Conroy¹, Sandro Tacchella^{3,4}, Joel Leja^{5,6,7}, Sam E. Cutler⁸, Benjamin D. Johnson¹, Erica J. Nelson⁹, and Razieh Emami¹

¹ Center for Astrophysics | Harvard & Smithsonian, 60 Garden St., Cambridge, MA 02138, USA; minjung.park@cfa.harvard.edu

² Dipartimento di Fisica e Astronomia, Università di Bologna, Via Gobetti 93/2, I-40129, Bologna, Italy

³ Kavli Institute for Cosmology, University of Cambridge, Madingley Road, Cambridge, CB3 0HA, UK

⁴ Cavendish Laboratory, University of Cambridge, 19 JJ Thomson Avenue, Cambridge, CB3 0HE, UK

⁵ Department of Astronomy & Astrophysics, The Pennsylvania State University, University Park, PA 16802, USA

⁶ Institute for Computational & Data Sciences, The Pennsylvania State University, University Park, PA 16802, USA

⁷ Institute for Gravitation and the Cosmos, The Pennsylvania State University, University Park, PA 16802, USA

⁸ Department of Astronomy, University of Massachusetts, Amherst, MA 01003, USA

⁹ Department for Astrophysical and Planetary Science, University of Colorado, Boulder, CO 80309, USA

Received 2022 October 6; revised 2023 March 29; accepted 2023 May 12; published 2023 August 9

Abstract

The existence of massive quiescent galaxies at high redshift seems to require rapid quenching, but it is unclear whether all quiescent galaxies have gone through this phase and what physical mechanisms are involved. To study rapid quenching, we use rest-frame colors to select 12 young quiescent galaxies at $z \sim 1.5$. From spectral energy distribution fitting, we find that they all experienced intense starbursts prior to rapid quenching. We confirm this with deep Magellan/FIRE spectroscopic observations for a subset of seven galaxies. Broad emission lines are detected for two galaxies, and are most likely caused by active galactic nucleus (AGN) activity. The other five galaxies do not show any emission features, suggesting that gas has already been removed or depleted. Most of the rapidly quenched galaxies are more compact than normal quiescent galaxies, providing evidence for a central starburst in the recent past. We estimate an average transition time of 300 Myr for the rapid quenching phase. Approximately 4% of quiescent galaxies at $z = 1.5$ have gone through rapid quenching; this fraction increases to 23% at $z = 2.2$. We identify analogs in the TNG100 simulation and find that rapid quenching for these galaxies is driven by AGNs, and for half of the cases, gas-rich major mergers seem to trigger the starburst. We conclude that these young massive quiescent galaxies are not just rapidly quenched, but also rapidly formed through a major starburst. We speculate that mergers drive gas inflow toward the central regions and grow supermassive black holes, leading to rapid quenching by AGN feedback.

Unified Astronomy Thesaurus concepts: [Galaxy formation \(595\)](#); [Galaxy evolution \(594\)](#); [Galaxy quenching \(2040\)](#)

1. Introduction

Star-forming activity is one of the fundamental characteristics of galaxies and is closely related to various properties, such as stellar mass, color, and morphology (e.g., Strateva et al. 2001; Baldry et al. 2004; Wuyts et al. 2011; Bluck et al. 2014). One of the most important unresolved questions in galaxy evolution is understanding how galaxies evolve from the star-forming to the quiescence phase. Several quenching mechanisms have been proposed, and recent studies have suggested two broad quenching processes with different timescales, namely “rapid” quenching and “slow” quenching (e.g., Wu et al. 2018; Belli et al. 2019; Wild et al. 2020). The post-starburst galaxies (PSBs), originally known as E + A galaxies (Dressler & Gunn 1983; Zabludoff et al. 1996), i.e., elliptical but with an A-type young stellar spectrum, are thought to be in rapid transition from star-forming to quiescence. As the name suggests, they are thought to have had starbursts in the past, but rapidly and recently quenched, so that they are still dominated by young stars, but without ongoing star formation (SF). Thus, these PSBs hold important clues about the rapid quenching processes (French 2021).

The origin of the starburst is not yet clear. Gas-rich major mergers have been suggested as a possible scenario (e.g., Barnes & Hernquist 1991; Bekki et al. 2005; Snyder et al. 2011). As galaxies undergo gas-rich mergers, gas can flow into the central region, triggering a starburst. However, it is not entirely clear whether mergers are always involved in this picture. Some studies have found evidence for merger-fueled central starbursts (e.g., Puglisi et al. 2019), while others suggest outside-in formation via dissipative collapse (e.g., Tadaki et al. 2017, 2020). At high redshifts, compaction processes driven by violent disk instability or misaligned gas streams could also trigger the central starburst (e.g., Dekel & Burkert 2014; Zolotov et al. 2015; Tacchella et al. 2016a; Nelson et al. 2019c). The central starburst will then deplete the gas temporarily, suppressing SF. Several studies have shown that galaxies could remain on the main sequence after significant central starbursts followed by gas compaction events (e.g., Tacchella et al. 2016a; Cutler et al. 2023; Ji & Gialalisco 2023). Therefore, some other preventive mechanisms are required to make galaxies remain quiescent.

Active galactic nucleus (AGN) activity seems to be an important mechanism for rapid quenching. It could both blow away gas (often referred to as kinetic feedback) and heat the surrounding medium and thus prevent cooling (thermal feedback). Many studies using simulations have shown that AGN activity is essential in reproducing post-starburst populations

(e.g., Pontzen et al. 2017; Davis et al. 2019; Zheng et al. 2020). However, it is very challenging to directly observe evidence of ongoing AGN activity. Several studies have shown that PSBs have emission diagnostics similar to LINERs (e.g., French et al. 2015). Galactic outflows have been observed for a number of PSBs (e.g., Baron et al. 2017; Maltby et al. 2019), and given their high speed ($>1000 \text{ km s}^{-1}$), the outflows are thought to be driven by ejective AGN feedback (e.g., Förster Schreiber et al. 2019).

At high redshifts, it is often very challenging to spectroscopically confirm PSBs, thus many studies focus on young quiescent galaxies (in many cases, photometrically selected), which are most likely to be recently and rapidly quenched (e.g., Whitaker et al. 2012a; Wild et al. 2016; Belli et al. 2019; Suess et al. 2020). Therefore, it is not clear whether these young quiescent galaxies had a starburst in the past and then rapidly quenched (thus, being truly “post-starburst”) or simply had a sudden quenching after a relatively flat star formation history (SFH; e.g., Wild et al. 2020). The fraction of quiescent galaxies that are young increases with redshift (Whitaker et al. 2012b; Wild et al. 2016; Belli et al. 2019), suggesting that the rapid quenching process seems to become more important and common at high redshifts. Several studies have also attempted to constrain the quenching timescales of galaxies, both in observations (e.g., Tacchella et al. 2022a) and simulations (e.g., Rodriguez-Gomez et al. 2019; Park et al. 2022), both at low and high redshifts. They found that galaxies at high redshifts tend to be more rapidly quenched (typically $<1 \text{ Gyr}$), while at low redshifts, they have a broad range of quenching timescales (up to several Gyr). The PSBs are also more frequently found at high redshifts ($>5\%$) than in the local Universe ($<1\%$; e.g., Wild et al. 2016), and the existence of quiescent galaxies found at very high redshifts ($z > 3$; e.g., Franx et al. 2003; Forrest et al. 2020), when the age of the Universe is less than a few Gyr, requires a very rapid quenching process. Indeed, D’Eugenio et al. (2020) studied nine spectroscopically confirmed quiescent galaxies at $z \sim 3$ and showed that their average spectra are very similar to those of PSBs.

However, it is not yet clear how much of the quiescent population was built up through the rapid quenching phase. Different studies have estimated how many quiescent galaxies have gone through the rapid quenching phase, and the conclusions are often sensitive to the definition of post-starburst and strongly depend on redshift. For example, Belli et al. (2019) identified rapidly quenched PSB galaxies as young quiescent galaxies with mean ages of 300–800 Myr and found that the contribution of rapid quenching to the buildup of the red sequence is $\sim 20\%$ at $z \sim 1.4$ and $\sim 50\%$ at $z \sim 2.2$. Wild et al. (2016) also used photometric data (using a supercolor selection) to identify post-starbursts and concluded that the post-starburst phase accounts for 25%–50% of the growth of the red sequence at $z \sim 1$. In summary, quite a significant fraction of quiescent galaxies can be explained by the PSB phase (e.g., Snyder et al. 2011; Wild et al. 2016; Dhiwar et al. 2023), especially at higher redshifts, highlighting the importance of the rapid quenching phase.

In this study, we focus on a population of young quiescent galaxies at $z \sim 1.5$ (with inferred mean stellar ages below 300 Myr), which has not been explored before, to understand the rapid quenching process at high redshifts and the significance of the rapid quenching phase in galaxy evolution. In Section 2, we describe the photometric data we use and how

we select 12 rapidly quenched candidates at $z \sim 1.5$ based on their rest-frame color. We also describe the Magellan/FIRE spectroscopic observation we conducted on a subset of our sample. In Section 3, we present results about their SFHs, sizes, and information we can learn from emission lines detected from spectroscopic observation. In Section 4, we estimate how many quiescent galaxies have gone through the rapid quenching phase, based on the crossing time of the rapid quenching region. In Section 5, using the TNG100 simulation, we identify rapidly quenched analogs and study what caused the starburst and rapid quenching at high redshifts. Finally, in Section 6, we discuss in more detail the size evolution of young quiescent galaxies and what it suggests, and also the possible physical mechanisms responsible for this rapid quenching, and discuss the overall picture of quenching at high redshifts. The summary and conclusion of our work is given in Section 7.

2. Data and Sample Selection

2.1. Selection of Rapidly Quenched Candidates from the UltraVISTA Catalog

At high redshifts ($z > 1$), it is very challenging to identify spectroscopically confirmed PSBs, as it requires much more time to detect the Balmer absorption lines that indicate the presence of young stellar populations. Therefore, we follow the method used in Belli et al. (2019), where they inferred the mean stellar ages based on the location in the *UVJ* diagram (i.e., rest-frame $U - V$ versus $V - J$ colors). We select the youngest quiescent galaxies with inferred ages $<300 \text{ Myr}$, which are the most likely to be rapidly quenched. Note that these galaxies are the youngest tail of the quiescent galaxies, carefully selected as potentially having a significant starburst and rapid quenching. Some of the slightly older (but still young) quiescent galaxies would have also been rapidly quenched, as shown in the work of Belli et al. (2019), where they studied young quiescent galaxies with inferred ages of 300–800 Myr. In the present work, we focus on this extremely young population (with inferred ages $<300 \text{ Myr}$) to investigate the rapid quenching phase more clearly. We describe below in more detail how we select the parent sample and our “rapidly quenched” candidates.

We use the COSMOS/UltraVISTA (UVISTA) catalog (Muzzin et al. 2013a) and select galaxies in the photometric redshift $1.25 < z < 1.75$ with $\log(M_{\text{stellar}}/M_{\odot}) \geq 10.6$. The redshift range is chosen so that the most important optical absorption and emission line features can be observed in the near-IR from the ground. We exclude objects that have $K_s > 23.4$, as they are likely to be point sources, and those having bad fits to their photometry ($\text{chi}^2 > 1.5$). Figure 1 shows the parent sample as gray triangles in the rest-frame *UVJ* diagram. The *UVJ* colors are from the UVISTA catalog, where the rest-frame colors are calculated with the EAZY code (Brammer et al. 2008). Following Belli et al. (2019), we use the rotated coordinates in the *UVJ* plane (see also Fang et al. 2018), defined as follows, which help us quantify the age trend along the diagonal direction:

$$\begin{aligned} S_Q &= 0.75(V - J) + 0.66(U - V) \\ C_Q &= -0.66(V - J) + 0.75(U - V). \end{aligned}$$

Then, the median stellar age of galaxies (t_{50}) can be inferred from the *UVJ* colors as follows: $\log(t_{50} \text{ yr}^{-1}) = 7.03 + 1.12 * S_Q$. Belli et al. (2019) calibrated this approximate relation

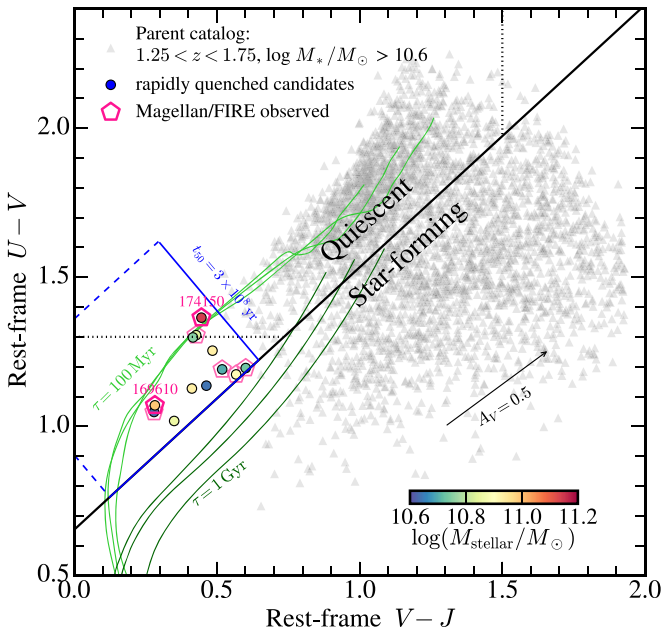


Figure 1. Rest-frame UVJ color-color diagram for selecting rapidly quenched candidates. The UVJ colors are from the UVISTA catalog, where the rest-frame colors are calculated with the EAZY code (Brammer et al. 2008). The gray triangles are the parent sample of massive galaxies ($\log(M_{\text{stellar}}/M_{\odot}) > 10.6$ at $1.25 < z < 1.75$) from the UVISTA catalog. The diagonal black line divides galaxies into quiescent and star-forming galaxies, and the dashed lines are additional constraints used in Muzzin et al. (2013b). The black arrow shows the effect of dust attenuation in the UVJ space, assuming the Calzetti et al. (2000) extinction law. We apply the method used in Belli et al. (2019) and identify 12 rapidly quenched candidates (the youngest non-star-forming galaxies), which are marked as filled circles and are color-coded by their stellar mass. We perform Magellan/FIRE observations of seven of these rapidly quenched candidates, marked as magenta pentagons. We highlight two galaxies, UVISTA 169610 and 174150, with their IDs, for which we have detected absorption features. The lime green and green lines are the evolutionary tracks for dust-free stellar population models with SFH exponentially declining with the e -folding timescales of 100 Myr and 1 Gyr, respectively. For each timescale, the three tracks correspond to three different values of stellar metallicity ($\log(Z/Z_{\odot}) = -0.2, 0.0, 0.2$).

using a spectroscopic sample with stellar ages older than 300 Myr. In this work, we aim at investigating rapidly quenched candidates, defined as the galaxies having $t_{50} < 300$ Myr and $C_Q > 0.49$ (quenched). The blue box in Figure 1 indicates the selection region for rapidly quenched galaxies (the dashed lines being arbitrary cuts).

Out of the 3595 objects in the parent sample, 12 galaxies satisfy our selection criteria. The 12 selected galaxies are shown in Figure 1 as filled circles, color-coded by their stellar mass (taken from Muzzin et al. 2013a). The lime green and green lines are the evolutionary tracks for dust-free stellar population models generated with the stellar population synthesis code FSPS (Conroy et al. 2009), assuming an exponentially declining SFH with e -folding timescales of 100 Myr and 1 Gyr, respectively. For each timescale, we show three tracks corresponding to $\log(Z/Z_{\odot}) = -0.2, 0.0, 0.2$. These tracks are generated with dust-free stellar models, and the presence of dust would shift each track toward the red (see the black arrow in Figure 1). This means that, at the location of each track, observed galaxies can be substantially younger and dustier than these simple models suggest. Thus the e -folding timescales of 100 Myr and 1 Gyr represent the upper bounds of the quenching timescales at each location. Indeed, the selected

12 galaxies are located between these evolutionary tracks, indicating that they are most likely quenched very rapidly.

We emphasize here again that our 12 “rapidly quenched” candidates are the youngest tail of the quiescent population, therefore they are most likely to have a major starburst and rapid quenching. However, they would not be the only galaxies that would have gone through rapid quenching. Some of the young (though slightly older than our sample) quiescent galaxies would have also been quenched rapidly, but they might have passively evolved for a few hundred Myr after quenching, or the degree of rapid quenching or the burstiness of the SF prior to it might not have been as strong as that of our sample. Our 12 rapidly quenched candidates are most likely to be in the stage immediately after the significant rapid quenching phase, best suited for the study of the rapid quenching phase.

2.2. Structural Data from 3D-DASH Survey

We use the data from the 3D-DASH survey (Mowla et al. 2022) to explore the morphology and sizes of our rapidly quenched UVISTA galaxies. The 3D-DASH program is a Hubble Space Telescope WFC3 F160W imaging and G141 grism survey targeting the COSMOS field, with an efficient Drift And SHift (DASH) observing technique (Momcheva et al. 2017). The global structural parameters for 3D-DASH, including Sérsic indices and sizes, are measured using GALFIT (Peng et al. 2002), identical to the methods in Cutler et al. (2022).

2.3. FIRE Observations and Data Reduction

We conducted the observations with a long-slit Echelle mode, generally using a $0''.6$ wide slit, which corresponds to a spectral resolution of $\sigma = 50 \text{ km s}^{-1}$, with a fixed position angle of 0° . For each observed galaxy, we aimed to have an exposure time of ≈ 4 hr, and we used the high-gain mode ($1.2e\text{-}/\text{DN}$). To improve the sky subtraction, we performed an A–B dithering mode for integration times of ≈ 900 s each.

The FIREHOSE pipeline¹⁰ was used for the data reduction, which traces the orders and applies flat-fielding, wavelength solution, illumination correction, and slit tilt correction. Some A0V stars close to the targets were observed for telluric correction, which was applied using the `xtellcorr` package (Vacca et al. 2003) implemented in FIREHOSE. The 2D spectrum is extracted from FIREHOSE for each A/B dithering position.

We were able to observe seven out of the 12 rapidly quenched galaxies; the observations are summarized in Table 1. In four cases, we detect a noisy stellar continuum but are unable to identify robust features. The lack of emission lines in these four cases suggests that the galaxies are not actively forming stars and are likely quenched. In the other three cases, we identify emission lines and/or absorption lines.

3. Results

3.1. SFH

3.1.1. Prospector Results Using Photometry Only

To explore the stellar population properties of the 12 selected galaxies to see if they had a starburst before rapid quenching

¹⁰ https://github.com/jgagneastro/FireHose_v2

Table 1
Summary of Magellan/FIRE Observations of the Seven UVISTA Galaxies among the 12 Rapidly Quenched Candidates

ID	$\log(M_*/M_\odot)$	H mag (AB)	z_{phot}	Observed	Exposure	Seeing	Emission	Absorption	z_{spec}
77854	10.70	20.6	1.34	2020 Feb	2.8 hr	$\sim 0''.6$	[N II], [O III]	...	1.333
199028	10.73	21.1	1.67	2020 Feb	2.5 hr	$0''.5\text{--}0''.6$
39507	10.83	20.6	1.52	2020 Feb	2.8 hr	$0''.8\text{--}1''.0$
24523	10.63	20.9	1.64	2021 Jan	2.5 hr	$\sim 0''.8$
169610	10.99	20.2	1.72	2021 Jan	4.0 hr	$0''.4\text{--}0''.6$	[N II] doublet	Balmer Series	1.7015
174150	11.14	20.2	1.72	2022 Feb–Mar	10.3 hr ^a	$0''.5\text{--}0''.8$	No emission	Balmer Series	1.7335
95964	10.91	20.4	1.50	2022 Mar	4.0 hr	$0''.5\text{--}0''.6$

Notes. Column (1): the ID from the UVISTA catalog. Column (2): stellar mass ($\log(M_*/M_\odot)$). Column (3): H -band magnitude (in AB). Column (4): photometric redshift (z_{phot}). Column (5): observed dates. Column (6): total exposure time. Column (7): seeing. Column (8): detected emission features. Column (9): detected absorption features. Column (10): the spectroscopic redshift (z_{spec}). Absorption lines are detected in only two galaxies: UVISTA 169610 and 174150. Those two galaxies are highlighted with their IDs in Figure 1.

^a Observed for three half nights. For the first two half nights, we used a $0''.6$ wide slit, and we switched to a $0''.75$ one on our last observing night. When combining these three-night data, we smoothed the data of the first two nights to $0''.75$ slit resolution ($\sigma = 62.5 \text{ km s}^{-1}$), then combined them with the third night’s data observed with a $0''.75$ slit.

(thus, whether they are truly “post-starburst”), we run *Prospector* (Johnson et al. 2021), a fully Bayesian stellar population inference code, to fit the photometric data released in the UVISTA catalog spanning from FUV to mid-IR (see Muzzin et al. 2013a for details about the photometric data of the UltraVISTA survey).

Prospector adopts the stellar population synthesis model FSPS (Conroy et al. 2009) to generate synthetic galactic spectral energy distributions (SEDs). We used MIST isochrones (Choi et al. 2016) and assume a Chabrier initial mass function (Chabrier 2003). The model consists of 19 free parameters describing the contribution of stars, gas, and dust. The nested sampling package Dynesty (Speagle 2020) allows us to efficiently sample from the parameter space based on given priors to estimate the Bayesian posteriors. The stellar population of a galaxy is described by a set of parameters, including redshifts, stellar mass, metallicity, dust parameters, and a nonparametric SFH (see more details about the setup for nonparametric models in Leja et al. 2019a, 2019b). Dust attenuation is modeled assuming two components, the birth-cloud component and the diffuse component, following Charlot & Fall (2000). The choice of the prior is very important as the fitting result is sensitive to it. We use a continuity prior for the nonparametric SFH, in which we assume that the ratio of the star formation rate (SFR) between two adjacent time bins follows a Student’s t -distribution with $\sigma = 0.3$ and $\nu = 2$ (Leja et al. 2019a). The use of a continuity prior favors a smooth variation of SFR between the two adjacent time bins and is thus biased against dramatic changes in SFR, such as rapid quenching or starbursts. See Tacchella et al. (2022b) and Suess et al. (2022) for more details about how the SFH reconstructed from the *Prospector* fitting would be changed when different priors are used. We used 14 time bins for nonparametric SFH, where the earliest bins are 30 and 100 Myr, beyond which the bins are evenly spaced in logarithmic ages. A constant SFR is assumed within each time bin.

Figure 2 shows the resulting SFHs for the 12 objects, reconstructed from *Prospector* fitting. The solid navy line shows the SFH from the maximum a posteriori (MAP) probability, and the shade represents 95% of the posterior distribution from 1000 random posteriors. Indeed, many of our sample galaxies are rapidly quenched with significant starbursts. UVISTA 166544 appears to be not fully quenched with

$\log(\text{sSFR}) \sim -9.4$. To quantify how rapidly our sample galaxies are formed, we measure the formation timescale (t_{50}^{90}), defined as the time it takes for a galaxy to increase its stellar mass from 50% to 90% of the final stellar mass. The orange horizontal bar in each panel indicates the formation timescale of each galaxy. The formation timescale we define here traces the second half of the formation history, which can be better constrained by the observations. Table 2 summarizes the *Prospector* fitting results and the formation timescales t_{50}^{90} . The average formation timescale of our 12 targets is $t_{50}^{90} = 320 \text{ Myr}$, which clearly shows that they are not just rapidly quenched, but also rapidly formed. We point out that this is a conservative result, because the continuity prior is biased against abrupt changes in the SFHs. The true formation timescales may be even shorter than the values we measure.

While fitting models to the photometric data gives us a rough idea of how rapidly galaxies are quenched, the detailed quenching history, as well as whether galaxies are truly quenched or showing any AGN signatures, can only be revealed with spectroscopic data.

3.1.2. *Prospector* Results Using Both Photometry and Spectroscopy

We detect clear absorption features for two galaxies, UVISTA 169610 and 174150—two of the most massive galaxies in our sample. To study their stellar population properties in more detail, we perform *Prospector* fitting again, using both the photometric data from the UVISTA survey and the spectroscopic data that we obtained from the Magellan/FIRE observations. When fitting a spectrum, the velocity dispersion of a galaxy is used as an additional free parameter. Fitting both photometry and spectroscopy requires calibration when combining the two sets of information; we follow the common approach of multiplying a polynomial function with the model spectrum to match the observed spectrum (see the details about spectrophotometric calibration in Johnson et al. 2021). The order of the polynomial is another additional free parameter and we set it to 10. For spectrum fitting, we mask out emission lines and bad pixels.

Figure 3 shows the Magellan/FIRE spectra of UVISTA 169610 (top) and UVISTA 174150 (bottom). The magenta lines in the left panels show the best-fit models from the *Prospector* fitting, which match both the spectra and the photometry, in physical units of $\text{erg s}^{-1} \text{ cm}^{-2} \text{ \AA}^{-1}$. The green

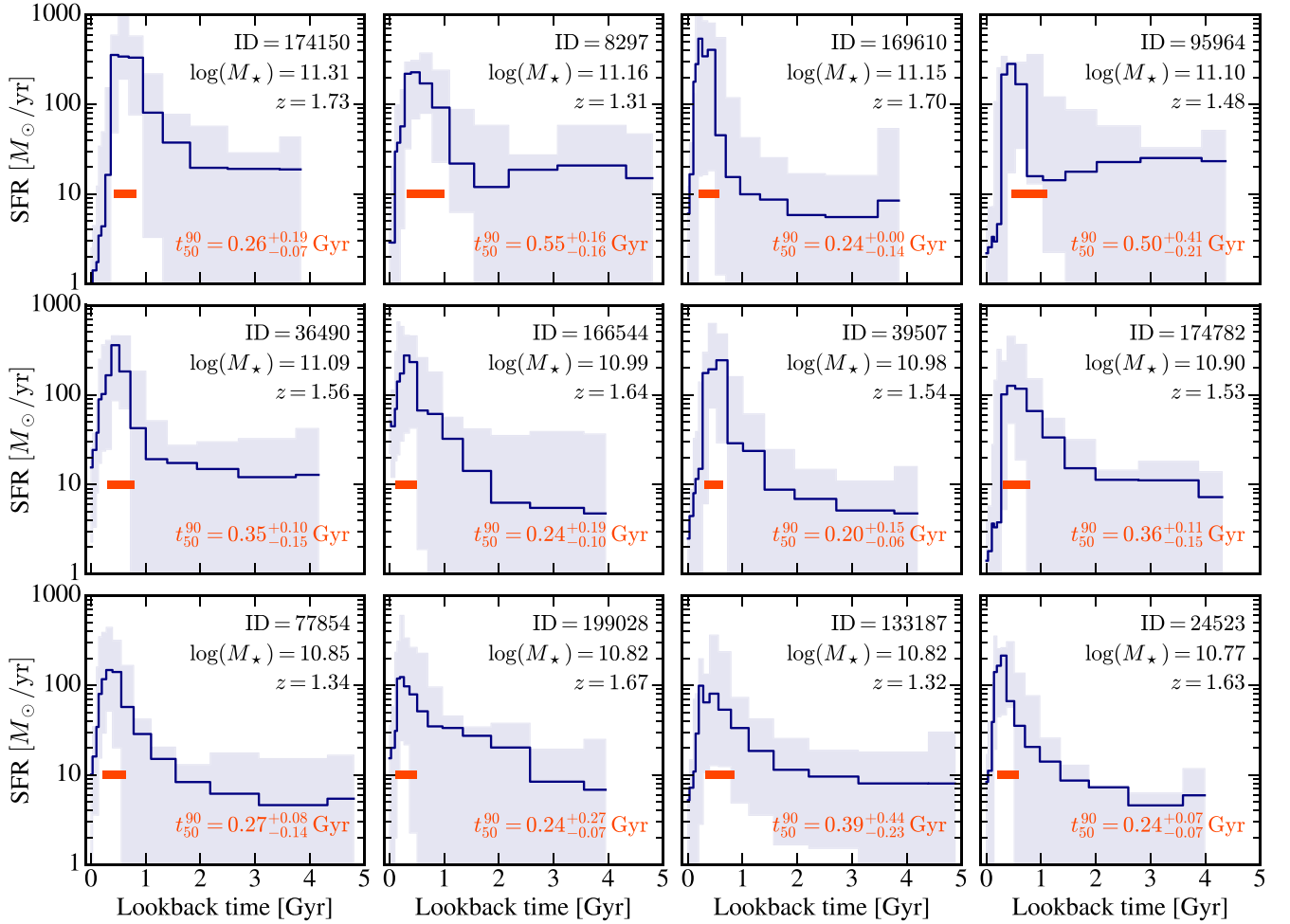


Figure 2. SFHs of 12 UVISTA galaxies derived from *Prospector* fitting on photometric data. The MAP distribution is shown as the solid navy line, while the shade indicates 95% of the SFH distribution from 1000 random posteriors. The orange horizontal bar indicates the formation timescales (t_{50}^{90} , the time it takes for the stellar mass of a galaxy to increase from 50% to 90% of the total stellar mass). We find that all of our 12 rapidly quenched candidates, solely selected based on their location in the *UVJ* diagram, are PSBs that are rapidly formed (with average formation timescale of $t_{50}^{90} \sim 320$ Myr).

lines are the observed spectra smoothed by a Gaussian with a width of 29 pixels ($\sim 15 \text{ \AA}$); in order to account for the necessarily imperfect flux calibration, the spectra are multiplied by a slowly varying polynomial so that their continuum matches the best fit. The gray windows are the wavelength regions dominated by skylines and/or large errors. Each panel on the right shows the resulting SFH. The MAP distributions are shown as red lines, with hatched regions indicating 95% of the posterior distributions. As a comparison, we include the posterior distribution when fitting the photometry only (the same as in Figure 2) as blue shaded regions.

The new fits yield SFHs that are consistent with those obtained without the spectra. The error bars of the SFH for UVISTA 169610 are significantly reduced when the spectroscopic data are included for fitting. On the other hand, in the case of UVISTA 174150, the SFH does not seem to be significantly improved with spectroscopic data. Older stellar populations, which are the hardest to measure, are slightly better constrained with spectroscopy, but the photometry alone seems to be able to do a good job in measuring the strength and duration of the main burst. Overall, for rapidly quenched galaxies where the Balmer break is strong, fitting only photometric data appears to be quite effective in constraining the SFH.

3.2. Sizes

The left panels of Figure 4 show the postage stamp images for the seven of the 12 UVISTA rapidly quenched candidates that are covered by the 3D-DASH survey. The redshift and the GALFIT fitting results for each galaxy, including the effective radius R_e and the Sérsic index $n_{\text{Sérsic}}$, are shown in the lower right corner of each panel. UVISTA 199028 is covered in the survey, but appears to be extremely compact, resulting in a bad fit using GALFIT.

The size–mass relations for six of our 12 UVISTA rapidly quenched candidates are shown in the right panel of Figure 4. UVISTA 199028, which has a bad GALFIT fit, is plotted as a dashed arrow. The red dashed line and the hatch region indicate the size–mass relation for (rest-frame *UVJ* color–selected) quiescent galaxies at $z = 1.75$ from van der Wel et al. (2014), while the relation for quiescent galaxies at $z = 1.25$ is shown as the red solid line and the shade. The relations presented in van der Wel et al. (2014) are fits to K-corrected “rest-frame” sizes. Thus, for consistency, we also correct the 3D-DASH sizes to “rest-frame” sizes, in the same way they did, using Equation (2) in van der Wel et al. (2014). Also in this plot, we use the stellar mass of the UVISTA galaxies provided by Muzzin et al. (2013a), which used the package *FAST* (Kriek et al. 2009), as in van der Wel et al. (2014). Broadly, the stellar masses of our

Table 2
Prospector Fitting Results of 12 UVISTA Rapidly Quenched Galaxies Based on Their Photometry

ID	$\log(M_*/M_\odot)$	z_{fitted}	$\log(Z/Z_\odot)$	$\hat{\tau}_{\text{dust},2}$	n	t_{50}^{90} (Myr)	R_{eff} (kpc)	$t_{\text{transition}}$ (Myr)
174150	$11.31^{+0.02}_{-0.02}$	1.73	$0.11^{+0.05}_{-0.09}$	$0.10^{+0.07}_{-0.04}$	$-0.32^{+0.31}_{-0.32}$	260^{+190}_{-70}	1.06 ± 0.03	308^{+41}_{-45}
8297	$11.16^{+0.03}_{-0.04}$	1.31	$0.00^{+0.11}_{-0.26}$	$0.05^{+0.03}_{-0.02}$	$-0.63^{+0.21}_{-0.19}$	550^{+160}_{-160}	...	243^{+115}_{-60}
169610	$11.15^{+0.01}_{-0.04}$	1.70	$0.05^{+0.10}_{-0.13}$	$0.14^{+0.07}_{-0.05}$	$-0.28^{+0.33}_{-0.19}$	240^{+0}_{-140}	...	t_{50}^{90}
95964	$11.10^{+0.01}_{-0.04}$	1.48	$-0.36^{+0.39}_{-0.21}$	$0.07^{+0.11}_{-0.05}$	$-0.49^{+0.27}_{-0.32}$	500^{+410}_{-210}	1.98 ± 0.22	414^{+48}_{-162}
36490	$11.09^{+0.03}_{-0.02}$	1.56	$0.10^{+0.06}_{-0.09}$	$0.29^{+0.05}_{-0.05}$	$-0.51^{+0.14}_{-0.19}$	350^{+100}_{-150}	...	154^{+53}_{-46}
166544	$10.99^{+0.06}_{-0.05}$	1.64	$-0.08^{+0.14}_{-0.48}$	$0.43^{+0.09}_{-0.08}$	$-0.12^{+0.14}_{-0.15}$	240^{+190}_{-100}	...	112^{+57}_{-70}
39507	$10.98^{+0.02}_{-0.02}$	1.54	$0.04^{+0.09}_{-0.10}$	$0.19^{+0.06}_{-0.06}$	$-0.58^{+0.27}_{-0.24}$	200^{+150}_{-60}	...	315^{+53}_{-63}
174782	$10.90^{+0.02}_{-0.03}$	1.53	$0.08^{+0.08}_{-0.12}$	$0.21^{+0.08}_{-0.07}$	$-0.57^{+0.26}_{-0.21}$	360^{+110}_{-150}	0.94 ± 0.13	235^{+60}_{-53}
77854	$10.85^{+0.03}_{-0.03}$	1.34	$0.13^{+0.04}_{-0.09}$	$0.40^{+0.06}_{-0.06}$	$-0.36^{+0.12}_{-0.12}$	270^{+80}_{-140}	1.14 ± 0.16	97^{+42}_{-36}
199028	$10.85^{+0.05}_{-0.03}$	1.67	$0.11^{+0.06}_{-0.18}$	$0.45^{+0.08}_{-0.10}$	$-0.44^{+0.09}_{-0.13}$	240^{+270}_{-70}	...	47^{+54}_{-26}
133187	$10.82^{+0.02}_{-0.03}$	1.32	$-0.33^{+0.13}_{-0.13}$	$0.17^{+0.05}_{-0.05}$	$-0.61^{+0.18}_{-0.23}$	390^{+440}_{-230}	3.05 ± 1.74	302^{+98}_{-77}
24523	$10.77^{+0.03}_{-0.03}$	1.63	$-0.02^{+0.15}_{-0.19}$	$0.15^{+0.04}_{-0.04}$	$-0.71^{+0.14}_{-0.13}$	240^{+70}_{-70}	0.86 ± 0.04	363^{+97}_{-75}

Notes. The galaxies are in descending order of stellar mass from the Prospector fits. Column (1): the ID from the UVISTA catalog; Column (2): stellar mass; Column (3): fitted redshift; Column (4): fitted metallicity; Column (5): the optical depth for the diffuse dust component (see details in Conroy et al. 2009); Column (6): the power-law modifier to the shape of the Calzetti et al. (2000) dust attenuation curve (see the details in Kriek & Conroy 2013); Column (7): the formation timescale (t_{50}^{90}); Column (8): the effective radius (R_{eff}); Column (9): rapid quenching transition time ($t_{\text{transition}}$, defined in Section 4.1) derived from the resulting SFHs.

12 rapidly quenched UVISTA galaxies are estimated to be 0.1–0.2 dex more massive when fitted by Prospector (see Leja et al. 2019b for a discussion of this effect). The gray horizontal line indicates the point-spread function (PSF) FWHM = 0".18 (converted into kiloparsecs at $z \sim 1.25$ – 1.75), below which the size of the galaxy might not be well resolved (the measured size being an upper limit).

Most of the seven UVISTA rapidly quenched galaxies are more compact than normal quiescent galaxies at their respective redshifts, consistent with the results of several previous works, where they found that young quiescent galaxies (or PSBs) tend to be more compact than old (or normal) quiescent galaxies (e.g., Whitaker et al. 2012a; Belli et al. 2015; Almaini et al. 2017; Maltby et al. 2018; Wu et al. 2018; Setton et al. 2022). There are two exceptions: UVISTA 95964 and 133187. The size of UVISTA 95964 is consistent with the relation of typical quiescent galaxies of the same redshift. UVISTA 133187 appears to have an extended structure, as shown in the left panel. A possible explanation for the extended structure is that this galaxy may be a rotating disk or have unresolved merging companions, but additional kinematic data are needed to confirm this. As a result of being compact, the Sérsic indices for these six galaxies are all quite high ($n_{\text{Sérsic}} > 2.5$). Their compact sizes, even more compact than normal quiescent galaxies, provide another piece of evidence that they had central starbursts before quenching, as we have confirmed from the Prospector SED fitting. We will discuss in more detail the possible physical mechanisms behind rapid quenching and compaction in Section 6.

3.3. Emission Lines

AGN activity is thought to play an important role in quenching massive galaxies, but it is very challenging to directly observe it. One of the most common ways to detect AGN activity is through emission line diagnostics. Many previous studies have shown that local PSBs mostly feature LINER-like emission lines (e.g., Yan et al. 2006; Wild et al. 2010; French et al. 2015; Alatalo et al. 2016)—although recently it has been pointed out that the low ionization is not necessarily centralized, suggesting that it might be caused by

post-AGB stars instead of AGN activity (e.g., Yan & Blanton 2012; Belfiore et al. 2016). At high redshifts, several studies have detected a broad emission component of H α and [N II] in many star-forming galaxies (e.g., Genzel et al. 2014; Förster Schreiber et al. 2019), which is thought to originate from the inner few kiloparsecs. With a very broad kinematics of FWHM ~ 1000 km s $^{-1}$, likely gravitationally unbound, these broad emission components are often associated with ejective AGN feedback.

We obtain the ionized gas spectra of UVISTA 169610 and 174150 by subtracting their best-fit stellar spectrum models from their calibrated observed spectra. Figures 5(a) and (b) show the resulting emission line complex of H α and [N II] $\lambda 6550, \lambda 6585$ of UVISTA 16910 and 174150. For UVISTA 169610, we fit six Gaussians to the ionized gas spectrum, accounting for both broad- and narrow-line components of H α , [N II] $\lambda 6550$, and [N II] $\lambda 6585$. The three narrow lines share the same width, and so do all the three broad lines. The flux ratio between [N II] $\lambda 6550 / \lambda 6585$ is fixed to be 0.326, following Förster Schreiber et al. (2019). We fitted for seven parameters: the width of the broad- and narrow-line components (σ_{br} , σ_{nr}), the line shift between the broad- and narrow-component centroids ($\Delta\lambda_{\text{shift}}$), and the flux of H α , [N II] $\lambda 6585$ for both broad- and narrow-line components (H α_{br} , [N II] $\lambda 6550_{\text{br}}$, H α_{nr} , [N II] $\lambda 6550_{\text{nr}}$).

It is clear that there is no ongoing SF in UVISTA 169610, as indicated by the very low level of H α emission; the measured H α flux is negligible compared to the [N II] flux. From the Gaussian fit of H α emission, we can set an upper limit to the SFR of UVISTA 169610, as SFR $< 0.07 M_\odot \text{ yr}^{-1}$, following the canonical correlation of Kennicutt (1998), and a lower limit on the ratio of [N II]/H $\alpha > 157.1$. The standard deviations of the broad- and narrow-line components are $\sigma_{\text{br}} = 707$ km s $^{-1}$ (FWHM $_{\text{br}} = 2.35\sigma_{\text{br}} = 1661$ km s $^{-1}$) and $\sigma_{\text{nr}} = 176$ km s $^{-1}$, respectively. The kinematics of the broad emission component suggests that the ionized gas outflow is gravitationally unbound, and thus most likely originating from AGN-driven outflows.

The derived ionized gas kinematics is very sensitive to the continuum fitting. For example, when we calibrate the observed spectrum to match the best-fit stellar spectrum using a

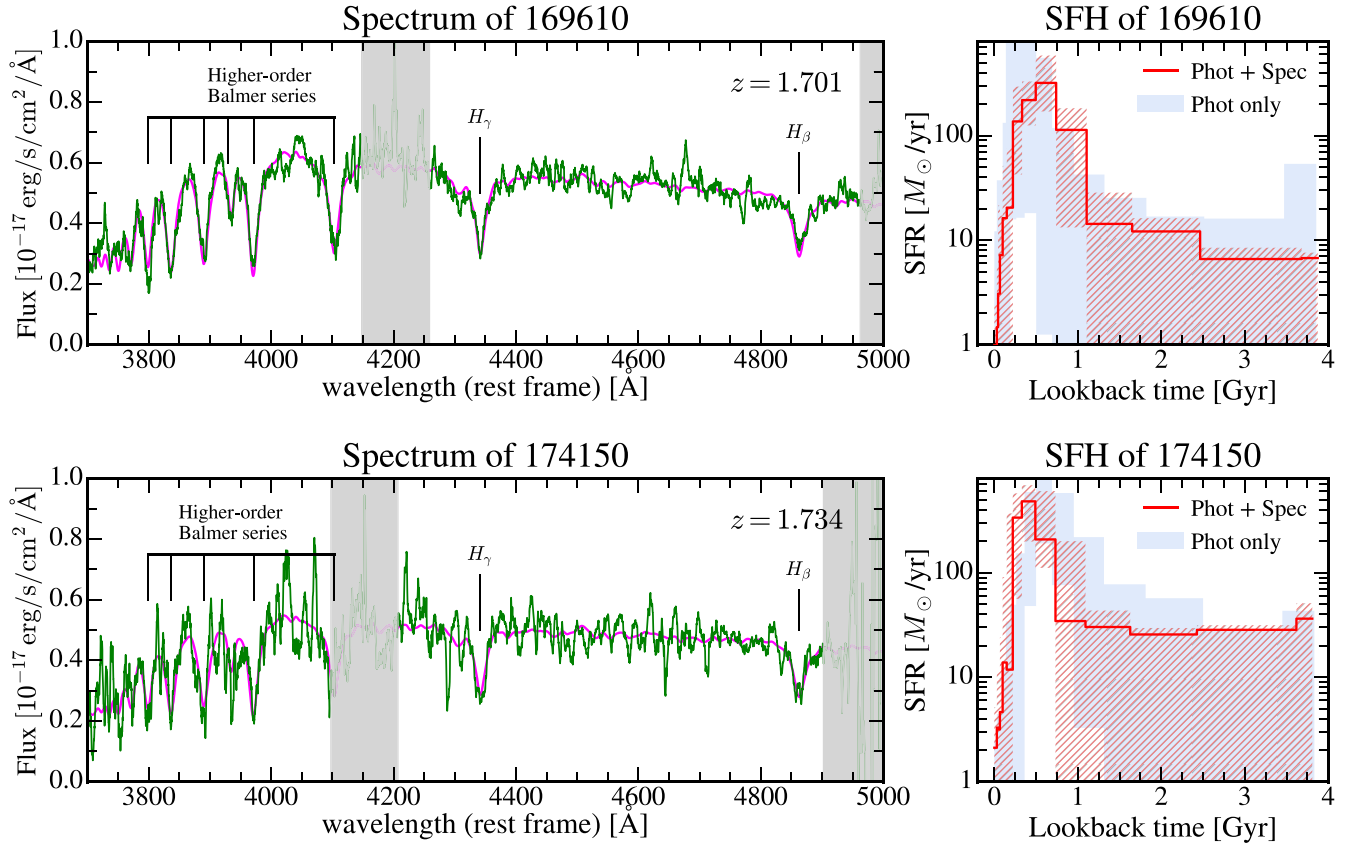


Figure 3. Magellan/FIRE spectroscopic data of UVISTA 169610 (top) and UVISTA 174150 (bottom). The smoothed data (smoothed with 29 pixels, corresponding to ~ 15 Å) are in green in both panels. The magenta lines show the best-fit stellar models from the `Prospector` fitting. The right panels show the resulting SFH of each galaxy. The red line shows the MAP distribution, and the hatched region includes 95% of the posterior distribution. The blue shade in the background shows 95% of the posterior distribution of SFH from `Prospector` fitting on photometric data only (the same as is shown in Figure 2). We confirm that both galaxies are rapidly formed with starbursts ~ 500 Myr before being rapidly quenched.

wavelength window that excludes absorption and emission lines, the fitted kinematics of the broad- and narrow-line components are $\sigma_{\text{br}} = 1200 \text{ km s}^{-1}$ and $\sigma_{\text{nr}} = 191 \text{ km s}^{-1}$. However, this does not change our conclusion that the broad-line component is most likely caused by AGN-driven outflows, because the SF in this galaxy is so suppressed (as indicated by extremely low $\text{H}\alpha$ emission) that it is very unlikely that the broad-line component is associated with SF outflows.

Interestingly, UVISTA 174150 does not seem to show any emission features, neither in $\text{H}\alpha$ nor in $[\text{N II}]$. The lack of $\text{H}\alpha$ emission can be explained by no ongoing SF, and the absence of $[\text{N II}]$ emission suggests that ionized gas may have already been blown away by the feedback processes.

We have also detected $[\text{N II}]$ and $[\text{O III}]$ emission lines for UVISTA 77854 (no Balmer absorptions detected due to high noise) and confirmed that the spectroscopic redshift is consistent with the photometric redshift. We perform the SED fitting on its photometric data using `Prospector` with fixed redshift ($z_{\text{spec}} = 1.333$) and assuming a fixed velocity dispersion of 200 km s^{-1} . The ionized gas spectrum is obtained by subtracting the best-fit stellar model from the spectrum, which is shown in Figure 5(c). We also fit the six Gaussians, in the same way as we did on UVISTA 169610. The resulting standard deviations of the broad- and narrow-line components are $\sigma_{\text{br}} = 400 \text{ km s}^{-1}$ ($\text{FWHM}_{\text{br}} = 2.35\sigma_{\text{br}} = 940 \text{ km s}^{-1}$) and $\sigma_{\text{nr}} = 131 \text{ km s}^{-1}$, respectively. The low level of $\text{H}\alpha$ emission (setting the upper limit of $\text{SFR} < 1.13 M_{\odot} \text{ yr}^{-1}$ and $[\text{N II}]/\text{H}$

$\alpha = 3.3$) suggests that the galaxy is indeed quenched and the ionized gas outflow most likely originated from AGN activity.

An interesting trend between the ionized gas content and the UVJ location can be found using these three galaxies (UVISTA 169610, 174150, and 77854), though more galaxies are needed to confirm the trend. Figure 5(d) highlights their UVJ locations with $[\text{N II}]/\text{H}\alpha$ ratios. Their SFHs are also shown in the inset panels with the logarithmic time axis. For UVISTA 169610 and 174150, the SFHs from the `Prospector` fits on both photometry and spectroscopy are shown, whereas the SFH of UVISTA 77854 is based on photometry fitting (all SFHs are in the same format: the MAPs are shown with solid lines, and the hatched or shaded area indicates 95% of the posteriors). UVISTA 169610, where $\text{H}\alpha$ emission is almost negligible, resulting in extremely high $[\text{N II}]/\text{H}\alpha = 157$, is indeed in the bluest corner of the UVJ diagram. UVISTA 77854 shows a non-negligible level of $\text{H}\alpha$ emission, setting the upper limit of $\text{SFR} < 1 M_{\odot} \text{ yr}^{-1}$, which is consistent with the estimated SFR from the `Prospector` fit. This galaxy is, indeed, closest to the star-forming region in the UVJ diagram. UVISTA 174150 is the reddest galaxy among our 12 rapidly quenched targets, and since it has low amounts of dust, its color is not likely reddened by dust (see the fitting parameter in Table 2). The SFH of this galaxy also suggests that it was quenched a few hundred Myr earlier than the other two galaxies, which might be related to the absence of ionized gas. While the other two galaxies still exhibit AGN-driven emission characteristics ~ 100 Myr after quenching, the ionized gas of UVISTA

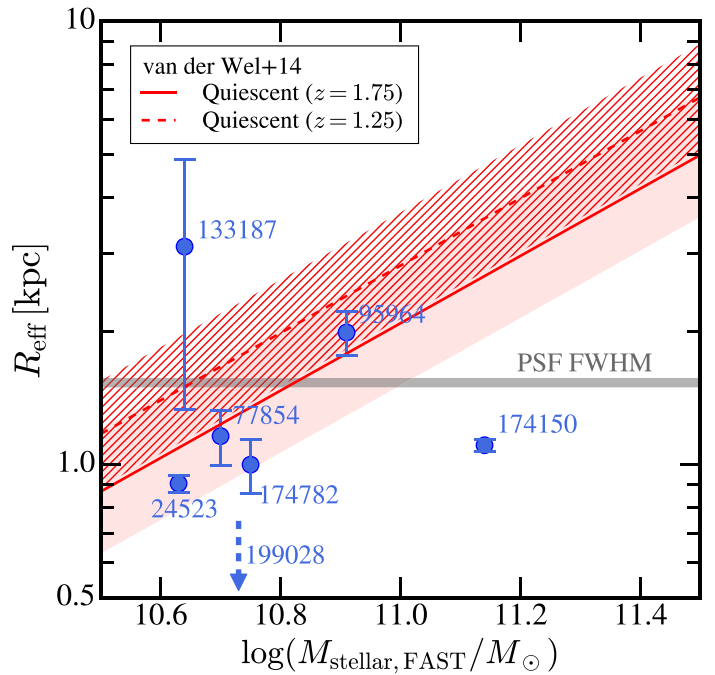
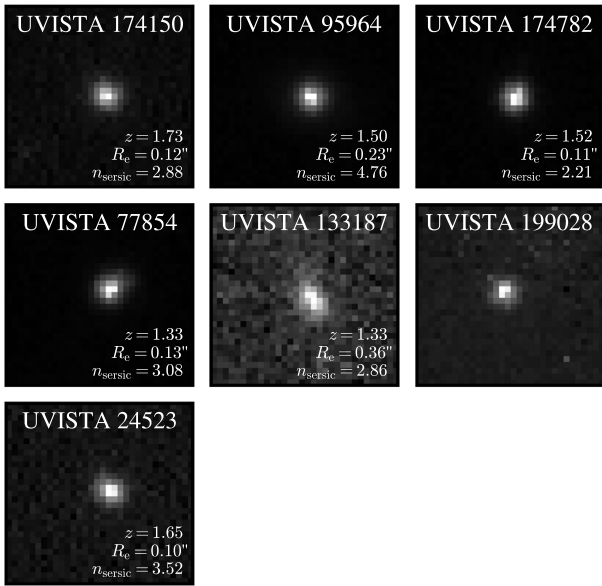


Figure 4. Left: 3D-DASH cutout images of seven of our 12 rapidly quenched candidates that are covered in the 3D-DASH survey. The box size is $3''$. The redshift of the galaxy (z), its effective radius (R_e), and the Sérsic index ($n_{\text{Sérsic}}$) are shown in lower right corner of each panel. UVISTA 199028 appears to be extremely compact, resulting in a bad fit using GALFIT. Right: size–mass relation for six of our UVISTA rapidly quenched candidates. UVISTA 199028 is plotted as a dashed arrow. The gray horizontal line indicates the PSF FWHM = $0.''18$, below which the size of the galaxy might not be well resolved (the measured size being an upper limit). The red dashed line and the hatch region indicate the size–mass relation for quiescent galaxies at $z = 1.75$ from van der Wel et al. (2014), while the relation for quiescent galaxies at $z = 1.25$ is shown as the red solid line and the shade. The stellar masses of the galaxies in this plot are derived using FAST, provided in Muzzin et al. (2013a), and the sizes are corrected to “rest-frame” sizes, to be consistent with van der Wel et al. (2014). We find that most of our UVISTA rapidly quenched candidates with size measurements seem to be more compact than normal quiescent galaxies at their respective redshifts.

174150 may have been all blown away ~ 300 Myr after quenching.

4. The Role of the Rapid Quenching Phase in the Buildup of the Quiescent Population

The “rapidly quenched” galaxies we select as the youngest quiescent galaxies, located at the bluest end of the quiescent sequence on the UVJ diagram, appear to be a rare population even at $z \sim 1.5$. However, they are experiencing a very rapid transition from star-forming to quiescence, and potentially hold important clues about the quenching process. Here, we measure how quickly galaxies transition this phase in the color space to estimate how many quiescent galaxies have gone through the rapid quenching phase.

4.1. Rapid Quenching Transition Time

To measure how quickly galaxies go through the rapid quenching phase, we explore the evolution of the rest-frame UVJ colors using the SFHs we obtained from the *Prospector* fitting. For each galaxy, we extract 1000 random posteriors from the *Prospector* fitting result and, for each posterior, we generate a stellar population using FSPS with the SFH, metallicity ($\log(Z/Z_\odot)$), $\hat{\tau}_{\text{dust},2}$, and n (dust index) values of the posterior in question. We then calculate the rest-frame UVJ colors of the stellar population generated for every time step. The time steps go beyond the observation epoch, to see how the colors of the rapidly quenched galaxies would evolve in the future (assuming that the galaxies remain fully quiescent).

Figure 6 shows the color evolution of one UVISTA galaxy in the UVJ diagram (left) and the SFH from the *Prospector* fitting that we used to calculate the colors (right). For visual purposes, we show the MAP SFH as a solid black line, and the UVJ color evolution based on it. Each colored point in both panels indicates a time step. Each gray line shows the SFH of each posterior and the resulting color evolution. The point with a thicker edge in the left panel shows the calculated UVJ colors at the observed epoch (lookback time=0), and the magenta star shows the UVJ colors provided by the UVISTA catalog; these are calculated with the EAZY code (Brammer et al. 2008), and may be slightly different from the ones obtained with *Prospector* (thick black edge).

The blue box in the left panel represents the region that we define as the “rapid quenching phase” ($C_q > 0.49$ and $t_{50} < 3 \times 10^8$ yr). For each of the 12 galaxies in our sample, we measure the time it takes to cross that region and define it as the (rapid quenching) transition time ($t_{\text{transition}}$). The inset panel shows the normalized probability density function (PDF) of $t_{\text{transition}}$ calculated with 1000 individual posterior samples, with each SFH and metallicity, $\hat{\tau}_{\text{dust},2}$, and n (dust index) fixed during the evolution. The median $t_{\text{transition}}$ of 1000 posterior samples for this object is $t_{\text{transition}} = 308^{+41}_{-45}$ Myr, and is shown as the blue vertical line in the inset panel, with the blue arrows indicating the 16th to 84th percentile range.

Figure 7 shows the measured transition times of all 12 UVISTA rapidly quenched galaxies. Each gray histogram shows the normalized PDF of the transition time of 1000 random posterior samples for each galaxy. The median timescale of 1000 random draws is shown in blue vertical lines, with a sky blue bar indicating the range from the 16th to

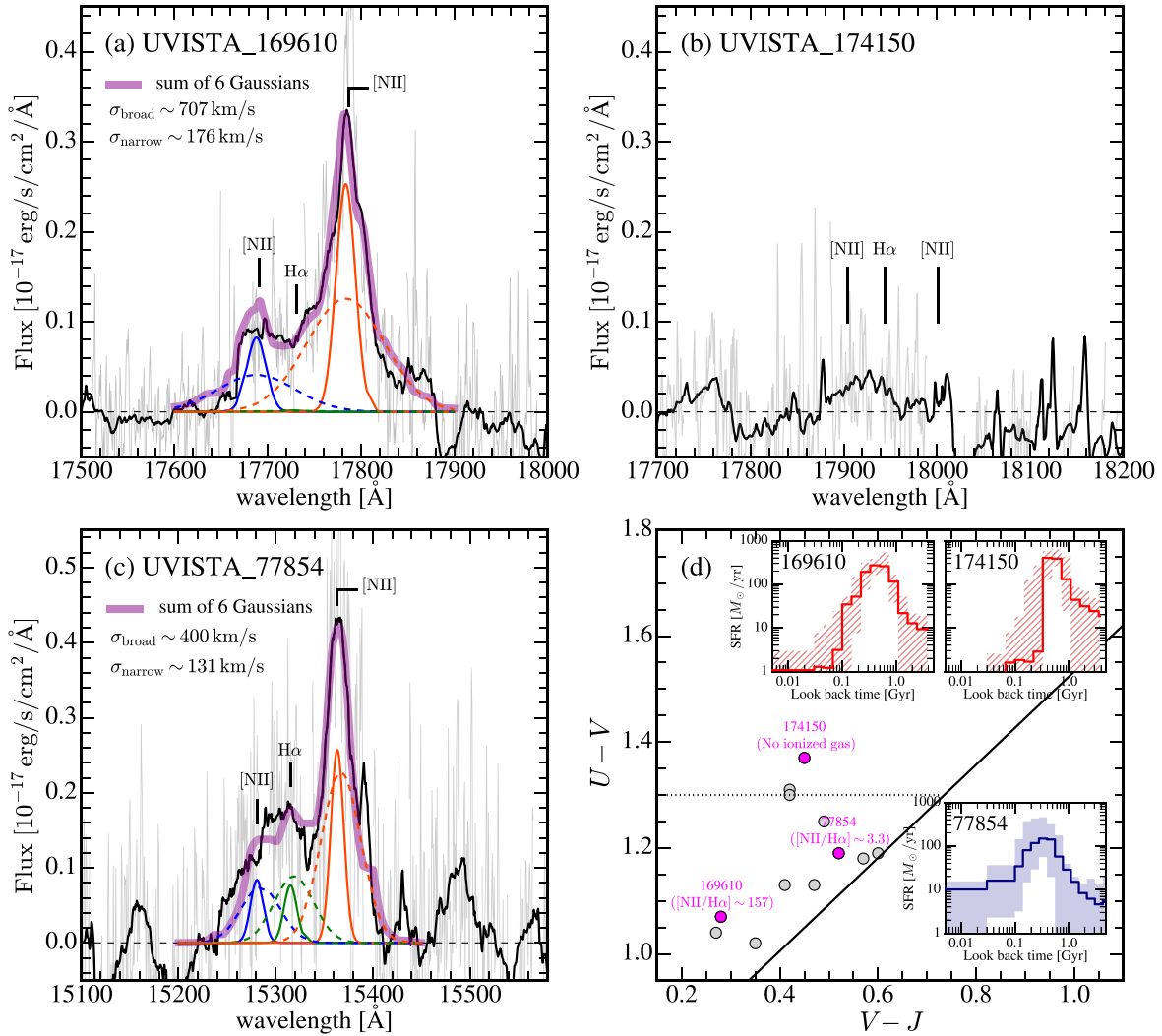


Figure 5. Ionized gas spectra of (a) UVISTA 169610, (b) UVISTA 174150, and (c) UVISTA 77854 around the H α , [N II] λ 6550, λ 6585 emission, in observed wavelength. The raw spectrum is shown in gray lines, and the black solid line in each panel shows the ionized gas spectrum smoothed with 29 pixels. For UVISTA 169610 and 77854, we fit six Gaussians to the ionized gas spectrum, accounting for both broad- (solid) and narrow- (dashed) line components of H α (green), [N II] λ 6550 (blue), and [N II] λ 6585 (orange). The thick purple line is the sum of the six Gaussians, smoothed in the same way as the observed spectrum. For UVISTA 169610, the fitted standard deviations of the broad- and narrow-line components are $\sigma_{\text{br}} = 707$ km s⁻¹ (FWHM_{br} = 2.35 σ_{br} = 1661 km s⁻¹) and $\sigma_{\text{nr}} = 176$ km s⁻¹, respectively. For UVISTA 77854, the fitted standard deviations are $\sigma_{\text{br}} = 400$ km s⁻¹ and $\sigma_{\text{nr}} = 131$ km s⁻¹. (d) The UVJ locations of the three galaxies and their SFH from *Prospector* fitting on a logarithmic time axis. We find that the ionized outflows found in UVISTA 169610 and 77854 are most likely driven by AGNs, given their high [N II]/H α ratios and the kinematics of the broad emission components (FWHM > 1000 km s⁻¹). UVISTA 174150, which is the reddest and quenched earlier, does not show any emission features, which might be because the AGN has already blown away all the ionized gas.

84th percentile. In the cases of UVISTA 199028 and UVISTA 166544, with some of their random posteriors, they end up not going through the rapid quenching phase region (the blue box in the left panel of Figure 6), but rather evolve by deflecting to the right corner of the region. This explains why the lower tail of their transition-time distributions seems to go below 0. For these two galaxies, therefore, we measure the median timescale only using the random posteriors with which they go through the rapid quenching region. The average (rapid quenching) transition time of the 12 rapidly quenched UVISTA galaxies is $t_{\text{transition}} = 250$ Myr. Excluding the three dust-rich galaxies, the average transition time is $t_{\text{transition}} = 305$ Myr. This estimate of the average transition time is likely an upper bound, given that we used fixed dust parameters during the evolution and the galaxies were almost certainly dustier before quenching. The true transition time may be even shorter than the values we measure.

For UVISTA 169610 and 174150, we measure the transition times using the SFH from the *Prospector* fitting on both photometric and spectroscopic data (i.e., the SFH presented in Figure 3). The green histogram shows the distribution of the transition times measured from 1000 random posterior samples, and the median and 16th to 84th percentiles are shown as green vertical lines and hatched bars. For UVISTA 169610, the median transition time is similar to that measured with the fit on photometric data only, yet the error bar is much better constrained with the spectroscopic data. On the other hand, the transition time of UVISTA 174150 is lowered when measured with the fit on both photometry and spectroscopy.

We find that dusty galaxies tend to have short transition timescales, as they cross only the right corner of the rapid quenching region (and, in some random posteriors, they do not even cross the region, as in UVISTA 199028 and 166544). This implies that very dusty rapidly quenched galaxies might have not been captured in our selection box, and our estimated

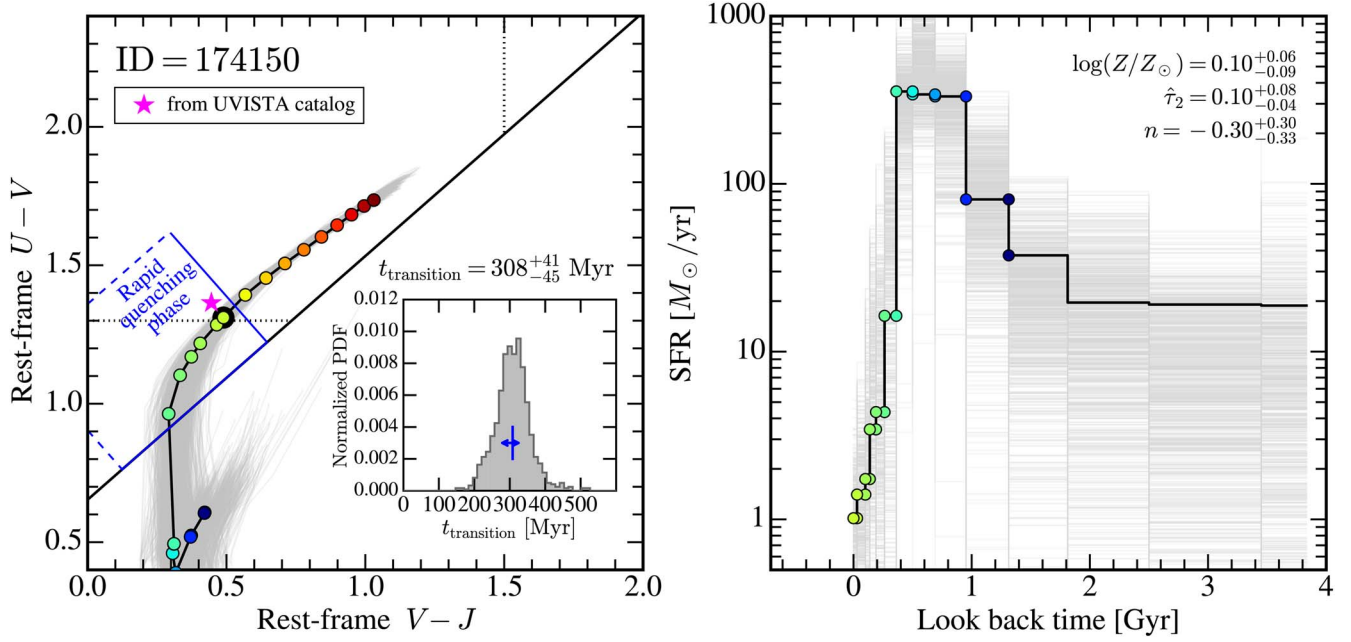


Figure 6. Left: rest-frame UVJ color evolution of UVISTA 174150. Right: SFH from *Prospector* fitting. In both panels, the results of 1000 random posteriors are shown as gray lines, and the black solid line shows the MAP for visual purposes only (not used for further calculations). Each colored point in both panels indicates a time step, including time steps that go beyond the observed epoch (the redder points show the future color evolution for the next 1 Gyr). The point with a thicker edge in the left panel shows the calculated UVJ colors at the observed epoch (lookback time = 0), and the magenta star shows the UVJ colors provided by the UVISTA catalog. From the *Prospector* fitting results (SFH and other stellar population parameters), we measure the time it takes for a galaxy to cross the rapid quenching region and define it as the rapid quenching transition time. For UVISTA 174150, the gray histogram in the inset panel on the left shows the distribution of the transition time measured with 1000 random posteriors, and the median time for this galaxy is $t_{\text{transition}} = 308^{+41}_{-45}$ Myr.

rapid quenching transition time holds true for relatively less dusty galaxies. The existence of dusty rapidly quenched galaxies also calls into question the implicit assumption that the amount of dust is a function of time, as they are assumed to be even dustier in the recent past (before quenching).

Figure 7(b) compares the transition time with the formation timescale t_{50}^{90} . The formation timescales, plotted as the orange horizontal line in Figure 2, indicate how rapidly galaxies are formed (the time including both the starburst and the rapid quenching phase). The transition time and formation timescales do not appear to be related, as they trace different processes, and also transition times are mostly affected by the amount of dust, as indicated by the color code.

Figure 7(c) compares the formation timescale with the quenching timescale. The quenching timescale here indicates how quickly SF subsides since starburst, defined as $t_{\text{SF peak}} - t_{\text{quench}}$, where $t_{\text{SF peak}}$ is the epoch when SF is at its peak and t_{quench} is the quenching epoch. The quenching epoch t_{quench} is defined as the time when the specific SFR (sSFR) drops below $\text{sSFR} = 1/[2 t_{\text{univ}}(z)]$, where $t_{\text{univ}}(z)$ is the age of the Universe (e.g., Tacchella et al. 2022a; Park et al. 2022). There seems to be a weak trend between the formation timescale and the quenching timescale; galaxies that are formed more rapidly with strong starbursts appear to be quenched more rapidly. The quenching timescale, however, does not correlate with the transition time shown as the color code.

In summary, the average (rapid quenching) transition time of our rapidly quenched UVISTA galaxies is $t_{\text{transition}} \approx 300$ Myr (excluding the three dust-rich galaxies with very short transition times). This estimate of transition is likely an upper bound, as we used fixed dust parameters during the evolution and galaxies were almost certainly dustier in the past. While the spectroscopic data seem to help constrain the transition time,

based on the two galaxies, the photometric data seem to be sufficient to estimate the transition time. More spectra are needed to determine exactly how many spectroscopic data will change the picture. The transition time seems to be related to the amount of dust (dustier galaxies tend to have shorter transition times), due to the shape of our selection box of the rapid quenching region, but not with how rapidly galaxies are formed (formation timescales). Note that the transition time itself does not hold any physical meaning, as can be seen from its weak correlation with the formation and quenching timescales. The purpose of measuring the transition time is to estimate the observability of the galaxies in this rapid quenching region and thus how many quiescent galaxies have undergone major starbursts and rapid quenching, which will be discussed in the following section.

4.2. Number Density

Based on the average rapid quenching transition time of $t_{\text{transition}} \approx 300$ Myr, we estimate how many quiescent galaxies have gone through this rapid quenching phase. In the same way as we selected the rapidly quenched (youngest quiescent) galaxies, we use the mean stellar age (t_{50}) inferred in Belli et al. (2019) to classify the quenched galaxies ($C_Q > 0.49$) into three populations:

1. $t_{50} > 800$ Myr: quiescent galaxies;
2. $300 < t_{50}/\text{Myr} < 800$: young quiescent galaxies (likely ‘‘PSBs’’); and
3. $t_{50} < 300$ Myr: the youngest quiescent galaxies (likely ‘‘burstier PSBs,’’ named ‘‘rapidly quenched’’ galaxies in this work).

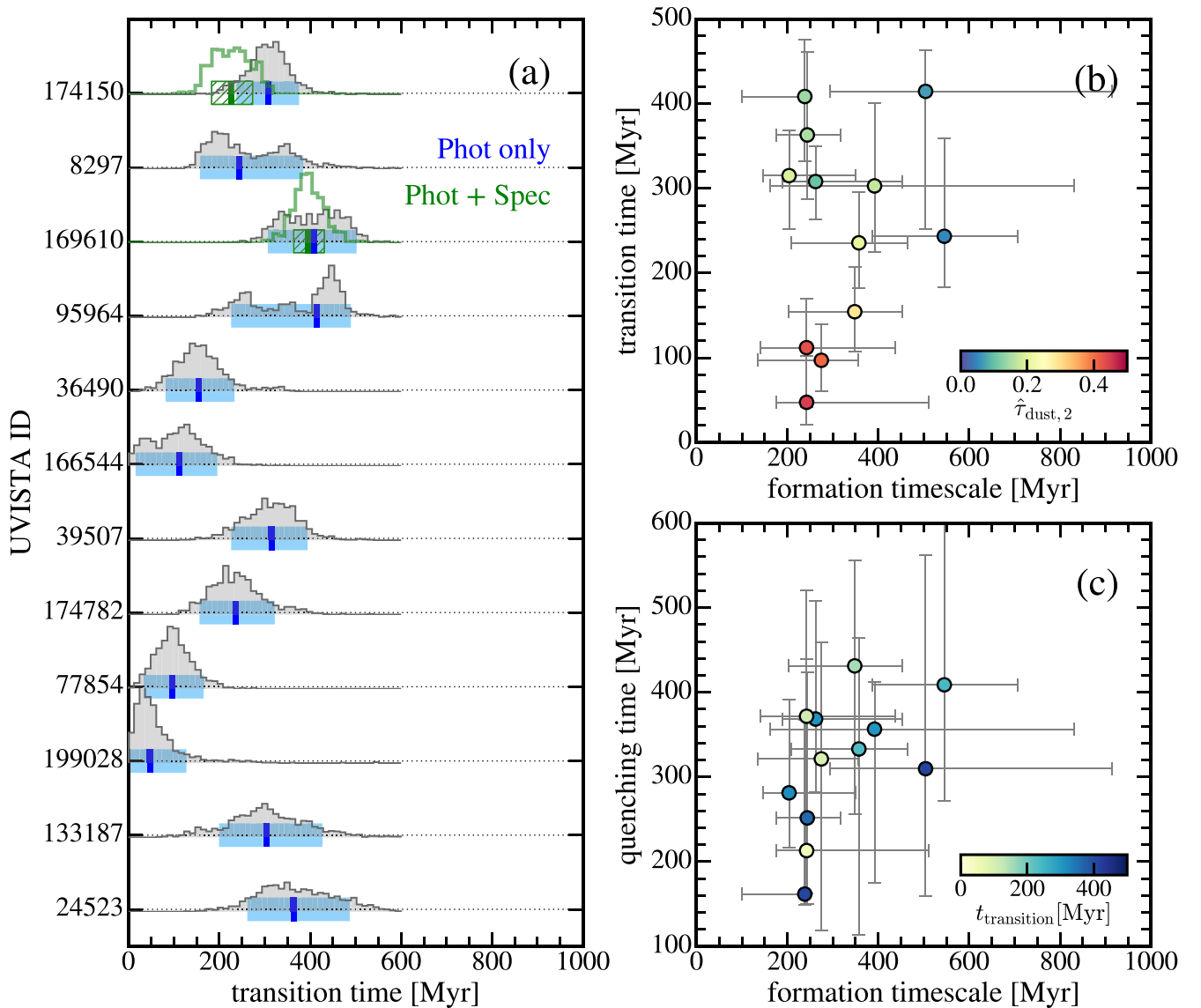


Figure 7. (a) Rapid quenching transition times of 12 UVISTA galaxies. The gray histogram shows the normalized PDF of the transition time of 1000 random posterior samples. The median timescales of 1000 random posterior samples are shown by the blue vertical lines, with a sky blue bar indicating the range from the 16th to 84th percentile. (b) Comparison between the transition time and the formation timescale (t_{50}^{PSB}). (c) Comparison between the quenching timescale and the formation timescale. We find that the average rapid quenching transition time of our samples is $t_{\text{transition}} \approx 300$ Myr and the transition time does not appear to be correlated with the formation or quenching timescales.

Note that the age cuts used for classifying these three populations are arbitrary. Especially, there is no clear distinction between the “PSBs” and the “rapidly quenched” galaxies. The rapidly quenched galaxies are likely the burstier tail of the PSB population.

Figure 8 shows the resulting quiescent (red), PSB (orange), and rapidly quenched galaxies (blue) in the UVJ diagram in four redshift bins that have the same comoving volume by construction. We apply the same mass cut ($\log(M_{\text{stellar}}/M_{\odot}) > 10.6$) for all redshift bins. The total number of galaxies in each redshift bin is shown in the upper left corner of each panel.

The top panel of Figure 9 shows how the number density of quiescent (red), PSB (orange), and rapidly quenched (blue) galaxies changes with redshift. While the number density of quiescent galaxies increases with time, the number density of PSB and rapidly quenched galaxies decreases significantly with time. This redshift trend of the number density of old and

young quiescent galaxies is consistent with previous work (e.g., Whitaker et al. 2012b; Wild et al. 2016; Belli et al. 2019). The growth rate of the quiescent population is calculated by the difference of their number densities in two adjacent redshift bins divided by the time interval between the two bins, and is plotted as the red circles in the bottom panel.

We calculate how much of the growth of the quiescent population can be explained by the transition of galaxies through the rapid quenching phase (assuming that the galaxies remain quiescent after quenching). This can be calculated by dividing the number density of rapidly quenched galaxies at the previous epoch by their transition time, which is $t_{\text{transition}}^{\text{rapid quenching}} = 300$ Myr. We calculate the contribution of the PSB galaxies to the growth of the quiescent population in an analogous way, assuming a transition time $t_{\text{transition}}^{\text{PSB}} \sim 500$ Myr (the time it takes for a passive evolution from $t_{50} = 300$ to 800 Myr), following Belli et al. (2019). Note that since rapidly quenched galaxies will eventually evolve into the PSB regions,

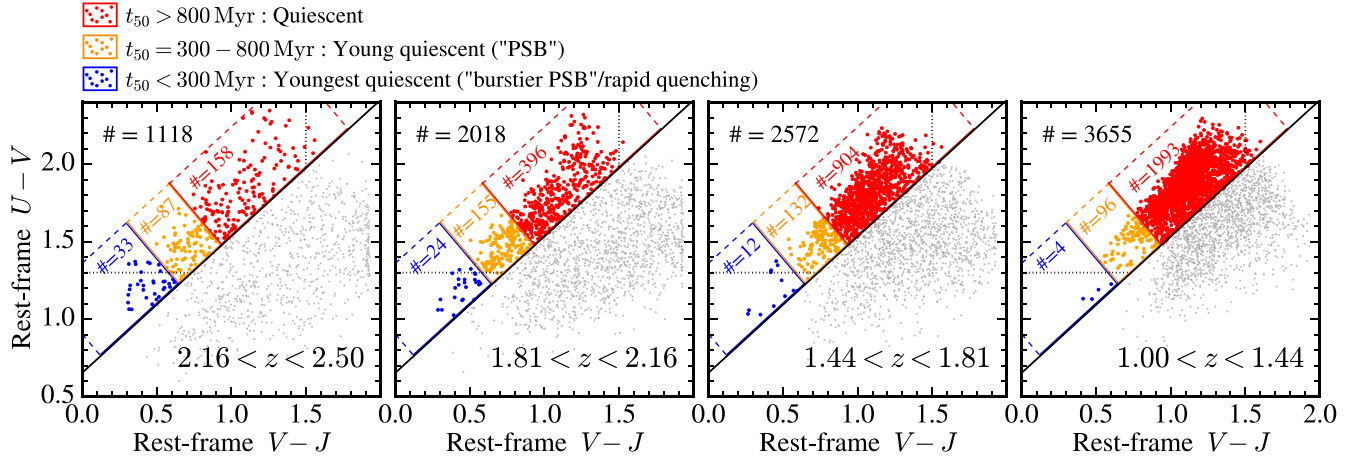


Figure 8. *UVJ* color-based identification of quiescent (red), PSB (orange), and burstier PSB/rapidly quenched (blue) galaxies in four redshift bins of equal comoving volumes. The color key on top of the figure describes how the three populations of galaxies are divided and named. The redshift range is shown at the bottom of each panel. The total number of galaxies in each redshift bin is shown in the upper left corner of each panel, and the number of galaxies in each population is displayed inside each selected region.

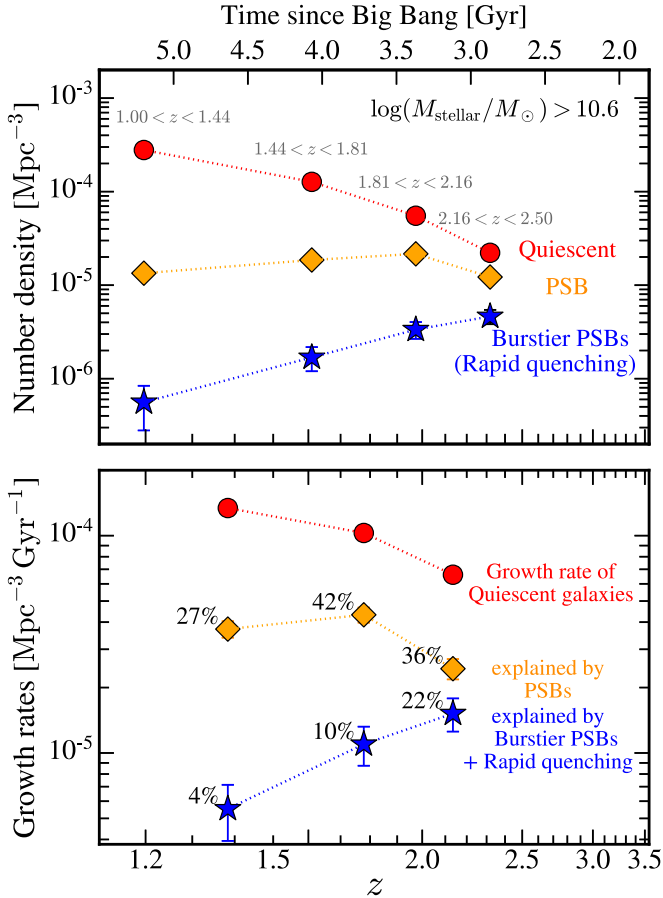


Figure 9. Top: number density of quiescent (red), PSB (orange), and rapidly quenched (blue) galaxies as a function of redshift. Bottom: growth rates of the quiescent population in red circles. The growth rates of the quiescent galaxies that can be explained by transitions from the PSB and the rapid quenching phases are plotted in orange diamonds and blue stars, respectively (percentages are displayed next to the symbols). We find that the fraction of quiescent galaxies that have gone through the rapid quenching phase increases with redshift: 4% at $z \sim 1.4$, 10% at $z \sim 1.8$, and 23% at $z \sim 2.2$.

the contribution rates of the PSB and the rapid quenching phases calculated here are inclusive.

The growth rates of the quiescent population that can be explained by the transition from the PSB and the rapid

quenching phases are plotted as orange diamonds and blue stars, respectively, in the bottom panel of Figure 9. Only 4% of the growth of quiescent galaxies can be explained by the transition from the rapid quenching phase at $z \sim 1.4$, suggesting that not many quiescent galaxies seem to have gone through this rapid quenching phase at this redshift. However, the rapid quenching phase seems to account for higher fractions of quiescent galaxies at higher redshifts (23% at $z \sim 2.2$). This is consistent with the fact that in the early Universe, galaxies need to be quenched rapidly in order to be identified as quiescent galaxies, given the short amount of available time. Indeed, several studies have found that the fraction of quiescent galaxies that had a strong starburst right before quenching increases with redshift (e.g., Setton et al. 2023). Recently, Noirot et al. (2022) have identified galaxies rapidly evolving from the blue cloud to the red sequence at $1.0 < z < 1.8$ (the “fast” population) and measured their quenching timescales. They found that the general population that has gone through the green valley (evolving on the “fast” tracks) is in complete agreement with the buildup of the quiescent population.

Several other factors could affect the population scatter, including the uncertainties in photometric redshift, dust, and metallicity. However, the impacts of the photometric redshift uncertainties and metallicity are not significant. Photometric redshifts are particularly accurate for the rapidly quenched galaxies because of the unique shape of the Balmer break, and metallicity does not affect their colors, as shown by the green tracks in Figure 1. Dusty rapidly quenched galaxies are missed due to dust reddening. There would be more rapidly quenched galaxies that did not fall into our selection box. Also, since we used fixed dust parameters during the color evolution, the rapid quenching transition time that we measured ($t_{\text{transition}} = 300$ Myr) is likely an upper bound. Therefore, the impact of dust would likely increase the estimated contributions of rapid quenching to the growth of the quiescent population.

Dry mergers of quiescent galaxies can also contribute to the growth rate of the quiescent population, which we have neglected in our analysis. The impact of dry mergers on the number density of a population can have two opposite effects; if the two (massive) galaxies in the selected quiescent population merge into one galaxy, the number density decreases, whereas a dry merger of two slightly less massive

galaxies results in one massive quiescent galaxy, which introduces a new galaxy in the population, thus increasing the number density. Belli et al. (2019) have assessed the impact of these two competing effects and concluded that the two effects almost cancel out for galaxies more massive than $\log(M_{\text{stellar}}/M_{\odot}) > 10.8$. Since we have used a similar mass threshold for our number density calculation, the effect of dry mergers would not affect our conclusion.

5. Rapid Quenching in the TNG100 Simulation

To understand what caused the starburst and rapid quenching at high redshifts in more detail, we use the TNG100 simulation to see if rapidly quenched analogs can be reproduced in simulations, and if they exist, to study how they are formed.

The TNG100 simulation, as part of the Illustris TNG project (Marinacci et al. 2018; Naiman et al. 2018; Nelson et al. 2018, 2019b; Pillepich et al. 2018; Springel et al. 2018), is a magnetohydrodynamical cosmological volume simulation run using the AREPO code. The box size of the simulation is ~ 100 Mpc (comoving), and the baryonic and dark matter (DM) mass resolutions are $m_{*} = 1.4 \times 10^6 M_{\odot}$ and $m_{\text{DM}} = 7.5 \times 10^6 M_{\odot}$, respectively. We use `hydrotools` (Diemer et al. 2017, 2018) to extract the data from the simulation.

Here we give a brief description about the feedback prescriptions implemented in the TNG models. Detailed descriptions can be found in Pillepich et al. (2018), Weinberger et al. (2017), Weinberger et al. (2018), and Pillepich et al. (2021). In the TNG models, stellar particles are formed in a gas cell where the density is above the threshold density of $n \simeq 0.1 \text{ cm}^{-3}$, following the Kennicutt–Schmidt relation (Springel & Hernquist 2003), and the Chabrier initial mass function (Chabrier 2003) is assumed for each stellar particle. As the stellar population evolves with time, it returns mass and metals into the surrounding medium by AGB winds (for stars with masses of $1\text{--}8 M_{\odot}$) and supernovae Type II ($8\text{--}100 M_{\odot}$) and Ia. A supermassive black hole (SMBH) with a mass of $\sim 10^6 M_{\odot}$ is seeded at the potential minimum of a halo more massive than $7.4 \times 10^{10} M_{\odot}$ and it grows either via SMBH–SMBH mergers or by accretion, following the Bondi–Hoyle accretion rate. The AGN feedback is modeled in two ways, depending on the accretion rate relative to the Eddington rate, and only one of the two modes is turned on at a time. When the accretion rate is high, thermal energy is isotropically and continuously injected into the surrounding medium (thermal or quasar mode), whereas when the accretion rate is low, feedback energy is injected in the form of kinetic energy in a pulsed and directed way (kinetic or wind mode).

There are in total 918 central galaxies with stellar mass $10.6 < \log(M_{\text{stellar}}/M_{\odot}) < 12.0$ at $z = 1.5$ in TNG100. Since dust is not included in the simulation, instead of *UVJ* colors, we select non-star-forming (or passive) galaxies, by applying the cut of $\text{sSFR} = 1/[2 t_{\text{univ}}(z)]$, where $t_{\text{univ}}(z)$ is the age of the Universe (e.g., Park et al. 2022; Tacchella et al. 2022a). We identify 50 quiescent central galaxies at $z = 1.5$ and measure their formation timescales (t_{50}^{90}). The left panel of Figure 10 shows the formation timescales (t_{50}^{90}) of all quiescent galaxies at $z \sim 1.5$ as a function of their quenching epoch, z_{quench} , defined as the epoch when their SFR starts to drop below $\text{sSFR} = 1/[2 t_{\text{univ}}(z)]$.

In Figure 9, we have estimated that $\sim 4\%$ of the growth of quiescent galaxies (i.e., 4% of the newly quenched galaxies) at $z \sim 1.5$ can be explained by the transition of the rapidly

quenched galaxies. The left panel of Figure 10 shows that there are only $\sim 5\text{--}6$ galaxies in TNG100 that are quenched at $z \sim 1.5$, and only 4% of them can be rapidly quenched analogs, according to our estimate. Indeed, these TNG100 galaxies quenched at $z \sim 1.5$ have much longer formation timescales. The formation timescales (16th–84th) of our 12 UVISTA rapidly quenched galaxies at $z \sim 1.5$ are shown as a blue hatched box for comparison.

Since there are too few rapidly quenched analogs quenched at $z \sim 1.5$, we instead select the 12 quiescent galaxies (regardless of quenching epochs) that have the shortest formation timescales; these are all quenched at earlier epochs. The 12 selected galaxies are marked with pentagons in the left panel and their SFHs are shown in the right panels. The green solid line shows the SFH derived from the age distribution of all stellar particles within $3 R_{\text{eff}}$, and the hatched gray histogram shows the SFH of stellar particles formed ex situ and later accreted. The formation timescales are shown as orange horizontal bars. The quenching epoch z_{quench} and the mass fraction of the stellar particles formed ex situ $f_{\text{ex situ}}$ are given in the right corner of each panel.

Clearly, in five of the 12 galaxies, (possibly gas-rich) major mergers seem to have triggered the starbursts. They have SF peaks shortly after the accretion of stars from other galaxies. On the other hand, the rest did not have major mergers, but still had starbursts and rapid quenching. This result is consistent with the results of Pathak et al. (2021), where they found that in TNG approximately half of the young quiescent galaxies at $z = 2$ have significant mergers prior to $z = 2$. They further found that those that had significant mergers have centrally concentrated young stellar populations, while the age gradient is rather flat for the young quiescent galaxies without mergers.

In all cases, the rapid quenching of massive quiescent TNG100 galaxies seems to be driven by kinetic AGN feedback. Many studies have shown that kinetic AGN feedback is responsible for quenching massive galaxies in the TNG model (e.g., Weinberger et al. 2018), while the energy injected via the thermal AGN mode is mostly radiated away, partially due to the limited numerical resolution, thus inefficient at quenching. We measure the epoch when the kinetic AGN mode is turned on for each galaxy and mark it with a magenta arrow in each SFH panel, and we can see clearly that the quenching epochs are tightly related to the epochs when the kinetic AGN mode is turned on.

6. Discussion

6.1. Size Evolution

Galactic morphology and sizes are closely linked to the SF activities of galaxies. In particular, star-forming and quiescent galaxies have distinct sizes at fixed mass, as found in many studies (e.g., van der Wel et al. 2014); at lower mass ($\log(M_{\text{stellar}}/M_{\odot}) < 10.5$), star-forming galaxies tend to be larger, with their extended star-forming disks, while quiescent galaxies likely develop centrally concentrated bulge-dominated structures, resulting in compact sizes. Therefore, the sizes of the galaxies are a reflection of how the structures have been transformed as the galaxies evolve to quiescence, holding an important clue of the physical mechanisms behind quenching.

The sizes of the newly quenched galaxies are expected to depend on their formation channel (e.g., Wu et al. 2018). If the

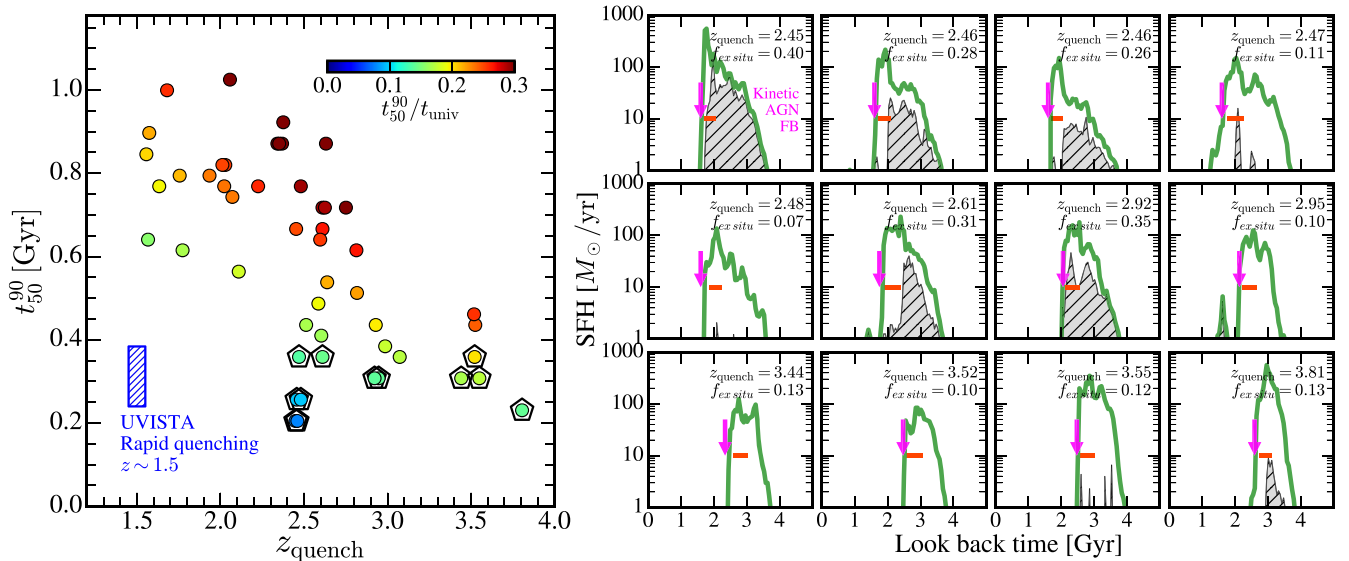


Figure 10. Left: formation timescale t_{50}^{90} of massive quiescent TNG100 galaxies ($10.6 < \log(M_{\text{stellar}}/M_{\odot}) < 12.0$) at $z \sim 1.5$ as a function of their quenching epoch (z_{quench}). Galaxies are color-coded by their t_{50}^{90} normalized by the age of the Universe at their quenching epoch. For comparison, the blue hatched bar indicates the 16th–84th percentile range of the t_{50}^{90} of 12 rapidly quenched UVISTA galaxies. We select 12 quiescent TNG100 galaxies that have the shortest t_{50}^{90} , marked with pentagons. Right: SFH of 12 TNG100 galaxies at $z \sim 1.5$ that are most rapidly formed. The green solid line shows the SFH derived from the age distribution of all stellar particles within $3 R_{\text{eff}}$, and the hatched gray histogram shows the SFH of stellar particles formed ex situ and later accreted. The formation timescales are shown as orange horizontal bars. The quenching epoch z_{quench} and the mass fraction of the stellar particles formed ex situ $f_{\text{ex situ}}$ are given in the right corner of each panel. We mark the epoch when the kinetic AGN feedback is turned on for each galaxy with the magenta arrows. It seems clear that kinetic AGN feedback is the key driver of the rapid quenching in TNG100. While major mergers appear to have triggered the starbursts in five of 12 rapidly quenched analogs in TNG100, the starbursts in the rest are likely triggered by other mechanisms not involving major mergers.

quenching mechanisms do not invoke significant structural changes, newly quenched (young quiescent) galaxies are expected to be similar or even larger as they are transformed from large star-forming progenitors (larger at later times). The possible quenching mechanisms include thermal AGN feedback that could heat the surrounding medium (e.g., Croton et al. 2006; Somerville et al. 2008) or very low SF inefficiency due to a bulge (e.g., Martig et al. 2009) or bar structures (e.g., Khoperskov et al. 2018). The addition of large newly quenched galaxies into the quiescent population can explain the size growth of the quiescent population with time. In this scenario, a clear size–age relation for quiescent galaxies is expected (e.g., van der Wel et al. 2009; Carollo et al. 2013; Fagioli et al. 2016). Dry minor mergers can complicate this picture, as they can also increase the size of galaxies by adding accreted stars to the outskirts of galaxies (e.g., van Dokkum 2005; Naab et al. 2007). On the other hand, if the quenching mechanisms involve dissipative processes that funnel gas into the central region and trigger a central starburst, this would result in smaller sizes than existing (old) quiescent populations. Several studies have also shown that these quenched galaxies after starbursts develop high central stellar mass densities (e.g., Tacchella et al. 2016a; Barro et al. 2017; Mosleh et al. 2017). Although, recently, Setton et al. (2022) have shown, based on the trend between sizes and the time since quenching, that the recent burst of post-starbursts would have taken place at larger (>1 kpc) spatial scales.

In Figure 4, we show the size–mass relations for six of our 12 UVISTA rapidly quenched galaxies, and most of them, except for one galaxy, have smaller sizes than the size–mass relations found at their respective redshifts. Our results are consistent with previous studies where they found that young quiescent galaxies (or PSBs) are more compact than older/normal quiescent galaxies (e.g., Whitaker et al. 2012a;

Belli et al. 2015; Almaini et al. 2017; Maltby et al. 2018; Wu et al. 2018). This supports the scenario in which significant structural changes, particularly compaction triggered by central starbursts, precede quenching for young quiescent galaxies, most commonly at high redshifts (e.g., Ji & Giavalisco 2022, 2023).

6.2. Physical Mechanisms Driving the Starburst and Rapid Quenching Phases

What are the physical mechanisms that quench galaxies rapidly while making them compact? One important finding from this work is that they are not just rapidly quenched, but also rapidly formed. As we have seen in Figure 2, all of our 12 UVISTA rapidly quenched candidates had intense starbursts a few hundred Myr before the observations, followed by rapid quenching. Their compact sizes (even more compact than normal quiescent galaxies, shown in Figure 4) also support the idea that gas flows into the central region, triggering starbursts in this limited region. At high redshifts, the compaction processes appear to be more common, and the possible mechanisms include mergers, violent disk instability, or misaligned gas streams (e.g., Zolotov et al. 2015; Tacchella et al. 2016a).

It is then reasonable to find the galactic gas being depleted after the starburst, but temporarily, as galaxies would be replenished with newly cooled gas from hot gas reservoirs. More sustainable feedback is required to keep PSBs quiescent. Many quenching mechanisms have been proposed; of these, mechanisms involving gas removal are thought to be rapid quenching process (e.g., Man & Belli 2018; Trussler et al. 2020)—for example, ejective AGN feedback (e.g., Silk & Rees 1998) or ram pressure stripping (e.g., Gunn & Gott 1972; commonly found in the cluster environment). Since at high redshifts environmental diversity is not as dramatic as in the local Universe, and the ram pressure stripping would be more

effective for smaller satellites with weaker restoring force, the ejective AGN feedback is the more likely scenario for the massive post-starbursts explored in this study.

Indeed, we have detected AGN-driven emission line characteristics for two of the three galaxies with spectral features detected (see Section 3.3). The kinematics of the broad components, $\text{FWHM} > 1000 \text{ km s}^{-1}$, suggest that these outflows are gravitationally unbound, and based on the very low level of $\text{H}\alpha$ emission, it is also very unlikely that the outflows are driven by SF. Also, in the TNG100 simulation, the rapid quenching seems to be caused by the kinetic AGN feedback, as explored in many previous studies (e.g., Weinberger et al. 2018; Nelson et al. 2019a; Luo et al. 2020; Terrazas et al. 2020); the quenching epochs of our rapidly quenched analogs are tightly related to the epoch when the kinetic AGN mode is turned on (see Figure 10).

Then, the question remains: what initiates the kinetic AGN feedback? Clearly, five of the 12 simulated rapid quenched analogs we explore in Figure 10 have (possibly gas-rich) major mergers ($f_{\text{ex situ}} > 0.25$) that trigger the starburst. The mass of the SMBH could have also significantly increased as a result of major mergers, releasing high amounts of kinetic energy to the surrounding medium and eventually leading to rapid quenching. On the other hand, for the rest of the galaxies in Figure 10 (especially galaxies that are quenched at higher redshifts, $z_{\text{quench}} > 3$), starbursts seem to be triggered by other mechanisms not involving major mergers, such as minor mergers or high rates of gas inflow. The gas inflow to the central regions that led to the starbursts could have fueled the SMBH and initiated the AGN feedback (e.g., Tacchella et al. 2016b).

In summary, the rapidly quenched galaxies at $z \sim 1.5$ are also rapidly formed with intense starbursts a few hundred Myr before quenching. The rapid quenching might be driven by the kinetic AGN feedback, as suggested by observed emission line characteristics (high $[\text{N II}]/\text{H}\alpha$ and the kinematics of broad emission components) and based on the quenching of TNG100 simulated galaxies. However, the dominant mechanism for the starburst is not clear. We have found some cases in which major mergers trigger the starburst, but in other cases, starbursts seem to require other mechanisms.

6.3. Overall Picture of Galaxy Quenching at High Redshift

As discussed in Section 4, the rapid quenching phase is a very short transition phase with a timescale of $\approx 300 \text{ Myr}$, and only a small fraction of quiescent galaxies (4% at $z \sim 1.4$ and $\sim 10\%$ at $z \sim 1.8$; see Figure 9) seem to have gone through this phase. Then, the question remains: what is the overall picture of galaxy quenching at high redshifts? To answer this question, we here explore the SFH of galaxies in other parts of the UVJ diagram. Moreover, by exploring galaxies outside our main selection, we check whether there is a substantial population of rapidly quenched galaxies we have missed because of high dust attenuation.

We measure the formation timescale of UVISTA galaxies in different regions of the UVJ diagram (see the selected regions, shown as boxes of different colors, in Figure 11). The galaxies in Figure 11 are color-coded by their formation timescale t_{50}^{90} . The parent sample is shown as gray circles in the background. Note that the number of galaxies where formation timescales are measured (thus, color-coded) in each selected region is arbitrary, for the purpose of finding a qualitative trend, so that the density distribution of the colored points does not represent

the density distribution of the parent sample. The right panels of Figure 11 show the SFHs of example galaxies in different regions (highlighted as diamonds in the left panel), derived from SED fitting on photometry using *Prospector*. The MAP distribution is shown as a solid line, with shades including 95% posterior distribution, and the colors of the lines represent the formation timescale of the particular galaxy. The formation timescale is also given as a horizontal bar in each SFH panel on the right.

It is clear that galaxies in different parts of the UVJ diagram have different formation timescales and SFHs. The galaxies in the rapid quenching region (as an example, the galaxy numbered “7,” named “Burstier PSBs”) are the ones that are the most rapidly formed (by very intense starbursts followed by rapid quenching), with formation timescales typically less than 0.5 Gyr. The galaxies in the PSB region are a mixture of galaxies similar to rapidly quenched galaxies (burstier PSBs) and others with less bursty SFH (an example is the galaxy numbered “4”). Quiescent galaxies have different quenching histories, depending on their location in the UVJ diagram, including galaxies that are rapidly quenched without having a starburst, thus having a rather flat SFH in the past (as in the galaxies numbered “1” or “2”), and galaxies that are slowly quenched (for example, galaxy “3”).

The majority of galaxies with the bluest $U - V$ colors (in the sky blue box region) have SFHs that are rapidly rising (galaxy “8”), and could be the progenitors of rapidly quenched galaxies, if their SF is abruptly terminated in the near future. Normal SF galaxies have a rather flat SFH (like galaxies “6” or “9”), and if they experience bursts in SF, they may evolve to the bluer side of the UVJ diagram (like galaxies “5” or “8”). On the other hand, if they are quenched, they will evolve into the quiescent region, like galaxy “1,” if quenched rapidly, and like galaxy “3,” if quenched slowly (see the Appendix for the recovery of rapid quenching in older galaxies).

A few galaxies in the quiescent and star-forming region of the UVJ diagram appear to have short formation timescales (colored as blue points in Figure 11). These are rapidly quenched but dust-rich galaxies, so they have much redder UVJ colors than the rapidly quenched galaxies we have selected. The existence of these dusty rapidly quenched galaxies will likely increase our estimated fractions of quiescent galaxies explained by the transition from rapid quenching in Figure 9. Among ~ 110 randomly selected quiescent galaxies we fit (out of the total number of ~ 1400 quiescent galaxies), only two are dusty rapidly quenched galaxies (burstier PSBs) with formation timescales less than 0.5 Gyr. We find that the number of dusty rapidly quenched galaxies is small compared to the overall population of quiescent galaxies. However, when considering the fact that we fit less than 10% of the quiescent population, it is possible that the total number of dusty rapidly quenched galaxies is comparable to or even larger than that of the dust-free, UVJ -selected galaxies. This means that our number densities of rapidly quenched galaxies may be underestimated by a factor of 2–3.

Figure 12 is a schematic diagram summarizing different evolutionary tracks from star-forming to quiescence in the UVJ diagram, depending on the SFHs. We show the UVJ color evolutions of galaxies that have a starburst followed by rapid quenching (blue), galaxies having less bursty SFH (green), and galaxies that do not have a starburst but simply have rapid (orange) and slow (red) quenching. For each case, the number

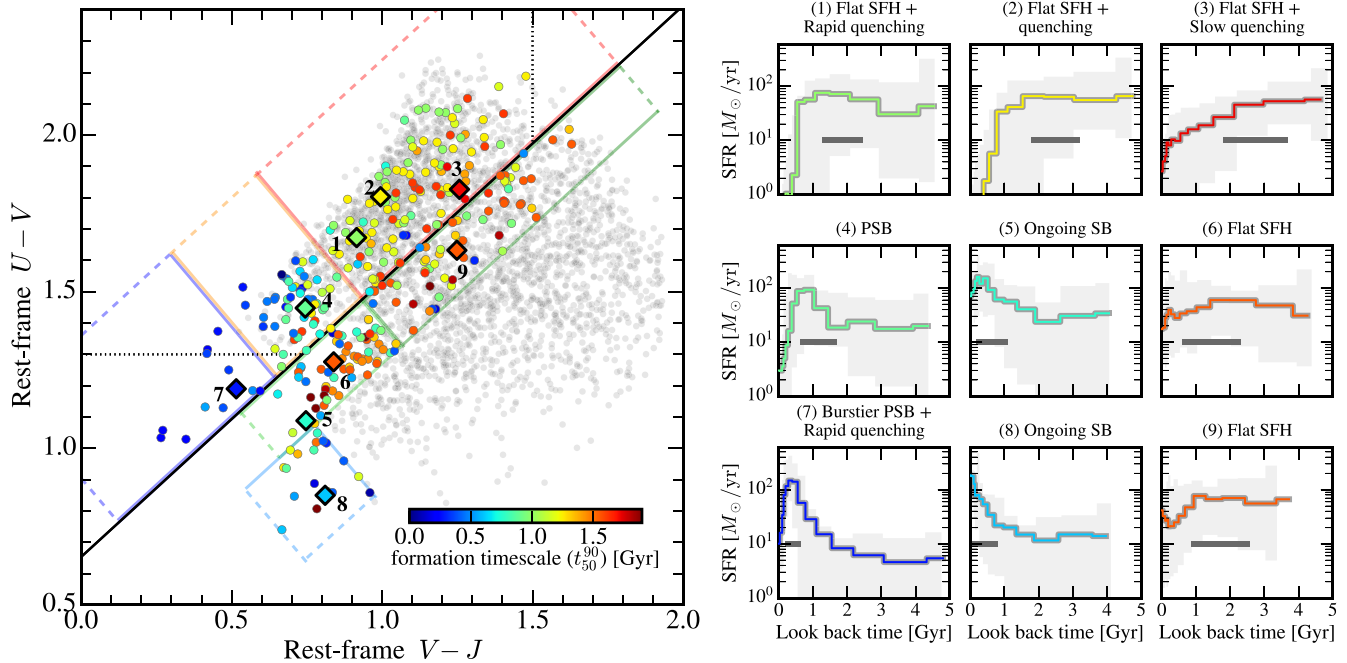


Figure 11. Formation timescale and SFH of UVISTA galaxies in different parts of the UVJ diagram. Left: UVISTA galaxies ($\log(M_{\text{stellar}}/M_{\odot}) > 10.6$ and $1.25 < z < 1.75$) in the UVJ plane, color-coded by their formation timescales. The parent sample is shown as gray circles in the background. Note that the number of galaxies where formation timescales are measured (thus, color-coded) in each selected region is arbitrary, for the purpose of finding a qualitative trend. Right: the SFHs of example galaxies in different regions (highlighted as diamonds in the left panel) derived from SED fitting on photometry using *Prospector*. The number at the top of each SFH panel corresponds to the diamond number on the left panel. The MAP distribution is shown in a solid line, with shades including 95% posterior distribution. The horizontal bar in each panel represents the formation timescale of each galaxy. We show that galaxies in different parts of the UVJ plane have different SFHs and thus different formation timescales.

in each colored circle in the UVJ space corresponds to the stage in SFH of that number in the right panel. The blue and red contours represent the regions that include 1σ and 2σ of massive ($\log(M_{\text{stellar}}/M_{\odot}) > 10.6$) star-forming ($C_Q < 0.49$) and quiescent ($C_Q > 0.49$) galaxies, respectively.

For galaxies that had starbursts in the past, the stellar mass would have also increased significantly during the starburst. Their star-forming progenitors before starburst (numbered “1”), therefore, have much smaller masses. We plot the distribution of slightly lower-mass galaxies ($9.8 < \log(M_{\text{stellar}}/M_{\odot}) < 10.6$) with the gray contour, and generally, lower-mass star-forming galaxies have much bluer colors. It is not clear how dusty these low-mass star-forming progenitors were, i.e., where they were located in the UVJ space, so we mark this part of the evolutionary track with dotted lines. As galaxies go through starbursts triggered by mergers and/or disk instability and become compact, they would evolve to the bluer corner of the UVJ diagram (numbered “2”). They would then evolve to the rapid quenching region as they are quenched (numbered “3”). The passive evolution after quenching (the track beyond point “3”) is plotted with dashed lines. If they have less extreme starbursts, they get only slightly bluer and are then quenched, as shown by the green track. Thus, only the galaxies that have extremely bursty SF followed by rapid quenching would end up in our rapid quenching region: the fraction of quiescent galaxies that would go through this extreme phase increases with redshift (see Section 4.2): 4% at $z \sim 1.4$, 10% at $z \sim 1.8$, and 23% at $z \sim 2.2$. Once they are quenched, they would passively evolve to the quiescence sequence shown by the red contour (dashed tracks).

Galaxies that do not experience starbursts would not evolve to the bluer side of the UVJ diagram, but their color would just get redder, as shown by the orange (rapid quenching) and red

(slow quenching) tracks. Because they are quenched without a starburst, their mass would not have increased much compared to before quenching. Thus, their star-forming progenitors before quenching most likely reside in the massive star-forming galaxy sequence, represented as the blue contour.

The evolution of the amount of dust has not been taken into account in this schematic diagram. Broadly, dust would move galaxies to the diagonal direction in the UVJ diagram, following the arrow, assuming the Calzetti et al. (2000) extinction law. As galaxies go through starbursts and rapid quenching, the amount of dust changes as well, but the detailed evolution is not entirely clear. There have been studies suggesting that the wide range of dust across the galaxies on the UVJ space could be entirely the effect of galaxy inclination (e.g., Zuckerman et al. 2021), which complicates the picture even more, since it links color evolution and morphological transformation. More detailed studies of the dust evolution during starburst and quenching, and how this evolution is related to inclination and morphology, are needed for future work.

The scenario outlined in Figure 12 is speculative. The four evolutionary tracks in the rest-frame UVJ color space depending on SFH would not be so clearly separated, due to dust evolution and morphological evolution, which have not been studied in this work; for example, $A_V = 0.5$ dust attenuation could easily smear out the differences between either the blue and green or the red and orange tracks. Nevertheless, one thing is clear; the young quiescent galaxies that are located on the bluer side of the UVJ diagram and would evolve on the blue or green tracks are not just rapidly quenched, but also rapidly “formed” with major starbursts. At higher redshifts, more quiescent galaxies

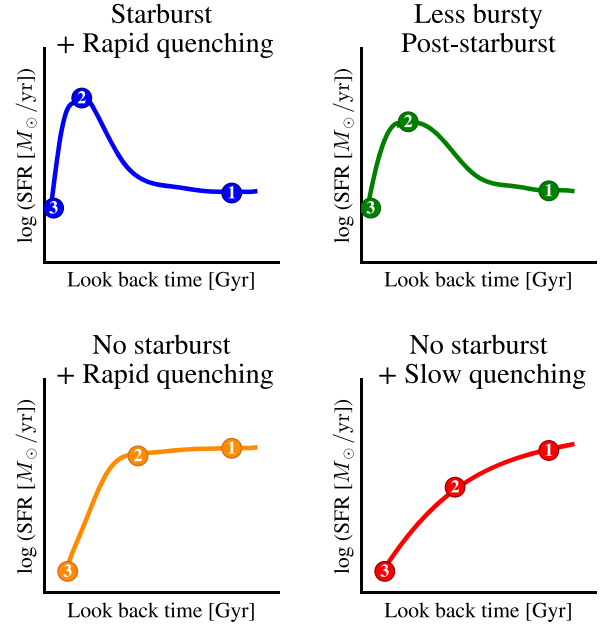
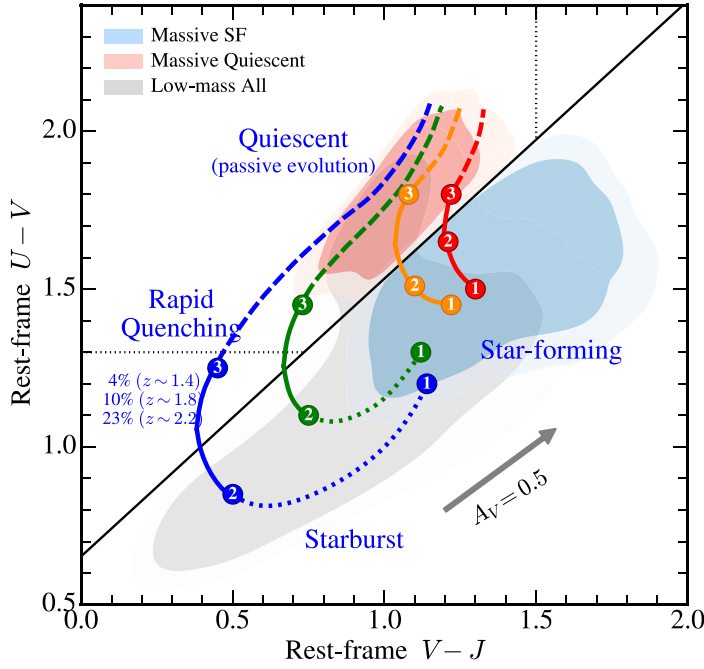


Figure 12. Schematic diagram summarizing different evolutionary tracks from star-forming to quiescence in the UVJ diagram, depending on the SFHs (blue: galaxies that have a starburst followed by rapid quenching; green: galaxies having less bursty SFH; orange: galaxies that do not have a starburst but simply have rapid quenching; and red: galaxies that are slowly quenched without a starburst). The numbers in each of the colored circles in the UVJ space correspond to the stage of SFH of the numbers in the right panel. The tracks for passive evolution after quenching are plotted by dashed lines. The blue and red contours represent the distributions of massive ($\log(M_{\text{stellar}}/M_{\odot}) > 10.6$) star-forming ($C_Q < 0.49$) and quiescent ($C_Q > 0.49$) galaxies, and the gray contour shows the distribution of lower-mass ($9.8 < \log(M_{\text{stellar}}/M_{\odot}) < 10.6$) galaxies.

would have gone through this starburst and rapid quenching before they become quiescent. Therefore, to understand quenching at high redshifts, we need to focus on the mechanisms that trigger not only the rapid quenching, but also the starbursts prior to it.

7. Summary and Conclusion

In this work, we have explored 12 young (< 300 Myr) massive ($\log(M_{\text{stellar}}/M_{\odot}) > 10.6$) quiescent galaxies at $z \sim 1.5$, selected based on their location in the UVJ diagram, as rapidly quenched candidates. Here we summarize our results.

1. From SED fitting of their photometric data using `Prospector`, we confirm that our young quiescent sample had intense starbursts in the past and then rapidly quenched (thus, they are truly “post-starburst”). They all formed very rapidly with a formation timescale (the time it takes to form 50% to 90% of their final stellar mass) of $t_{50}^{90} \approx 320$ Myr (Figure 2). Using the 3D-DASH data, we find that most of the sample have compact sizes, even smaller than normal quiescent galaxies (Figure 4). Their compact sizes provide another piece of evidence that they had central starbursts in the past.
2. We performed Magellan/FIRE spectroscopic observations of seven galaxies, and we confirm that they are truly quenched without $H\alpha$ emission. We detected absorption lines for two of the most massive galaxies in our sample (UVISTA 169610 and 174150) and found that their quenching history is slightly better constrained with the spectroscopic data, but the photometric data seem to be sufficient to provide an estimate of how rapidly galaxies are quenched. Of the three galaxies with spectral features,

two of them show signs of AGN activity, with high $[N\text{ II}]/H\alpha$ ratios and broad emission components ($\text{FWHM} > 1000 \text{ km s}^{-1}$). The other galaxy, the reddest galaxy among our sample, does not show any emission features, suggesting that ionized gas may have already been blown away by AGN activity.

3. From the SFHs of the 12 UVISTA galaxies, we infer the time it takes to cross the rapid quenching region, finding a transition time of ≈ 300 Myr. Using this transition time, we calculated how much of the growth rate of quiescent galaxies can be explained by the transition from rapid quenching and found that the rapid quenching phase accounts for only a small fraction of the growth of the quiescent population at $z \sim 1.5$. However, the fraction of quiescent galaxies that have gone through the rapid quenching phase increases with redshift: 4% at $z \sim 1.4$, 10% at $z \sim 1.8$, and 23% at $z \sim 2.2$ (Figure 9).
4. We identified 50 massive quiescent galaxies ($10.6 < \log(M_{\text{stellar}}/M_{\odot}) < 12.0$) at $z \sim 1.5$ in the TNG100 simulation and measured their formation timescales. We found that galaxies quenched earlier are formed more rapidly and selected the 12 galaxies that have the shortest formation timescales. In five of these 12 galaxies, starbursts appear to have started shortly after major mergers, while the others did not have major mergers, but still had starbursts and rapid quenching. In all cases, the rapid quenching in TNG100 is driven by the kinetic AGN feedback.
5. We studied the SFHs of galaxies in other parts of the UVJ diagram from the `Prospector` fitting on their photometric data and found that their formation timescales and histories depend on the location in the UVJ diagram. We show how galaxies would evolve in the UVJ space when

they have/do not have a starburst and when they are rapidly/slowly quenched (Figure 12).

The mechanisms by which high-redshift galaxies in the early Universe stop forming stars and become quiescent remain a puzzle. Based on our study of the youngest quiescent galaxies at $z \sim 1.5$, we conclude that these massive quiescent galaxies quenched at high redshifts are not just rapidly quenched, but also rapidly formed with a starburst. The starburst appears to have occurred in the central regions, given their compact sizes, likely triggered by dissipative processes such as gas-rich mergers, migration of star-forming clumps, or accretion of gas streams. In the TNG simulation, rapid quenching is driven by SMBH feedback that has grown as a result of the processes that led to central starbursts prior to rapid quenching.

The importance of rapid quenching becomes more significant at higher redshifts, as we estimated in this work. In particular, at high redshift ($z > 3$), where the age of the Universe is less than 2 Gyr, all of the quiescent galaxies are expected to be quenched rapidly. We expect that future observations using, e.g., JWST, of the first quiescent galaxies in the early Universe will shed more light on our understanding of the rapid quenching and further galaxy evolution. Also, future simulations that use realistic AGN feedback models and have sufficient resolutions to resolve AGN jets and central starbursts will help us understand the detailed sequential process of the rapid formation at high redshifts.

Acknowledgments

We thank Dylan Nelson and Annalisa Pillepich for useful discussions. S.B. is supported by the Italian Ministry for Universities and Research through the Rita Levi Montalcini program. C.C. acknowledges support from NSF AST-1908748. S.C. wishes to acknowledge funding under HST-GO-16259. R. E. acknowledges the support from the Institute for Theory and Computation at the Center for Astrophysics, as well as grant

numbers 21-atp21-0077, NSF AST-1816420, and HST-GO-16173.001-A, which provided very generous support.

Appendix

How Does the Derived SFH of Rapidly Quenched Galaxies Change after Passive Evolution?

Figure 11 shows the continuous distribution of quiescent galaxies with a clear age trend along the diagonal direction: from youngest quiescent galaxies that are rapidly and recently quenched to old quiescent galaxies. Once galaxies are quenched, they will passively evolve along the diagonal direction of the UVJ diagram. Thus, the old quiescent population consists of galaxies that have passively evolved after rapid quenching in addition to galaxies that are slowly quenched. In Section 4.2, we calculated how much of the growth rate of the quiescent population can be explained by the transition from rapid quenching and found that only a small fraction of quiescent galaxies appear to have gone through the rapid quenching phase ($\approx 4\%$ at $z \sim 1.4$). We aim to confirm this finding by checking directly how the SFH from the Prospector fitting would change as galaxies passively evolve. In this section, we test what the SFH of rapidly quenched galaxies would look like if they were observed a few Gyr later and compare it with the SFH of old quiescent galaxies.

To take into account the passive evolution, we push back the SFH of a rapidly quenched galaxy and remove the oldest bins so that we can still assume that the galaxy is observed at the same redshift. The right panel of Figure A1 shows the MAP SFH of UVISTA 174150 (blue) and the SFH pushed back by 0.5 Gyr (green), 1 Gyr (orange), and 2 Gyr (red). We then generate a stellar population using FSPS by feeding each SFH and calculate the magnitudes (flux) for the UVISTA photometric filters. We assume the same signal-to-noise ratio of the photometric measurements for each filter used in the UVISTA

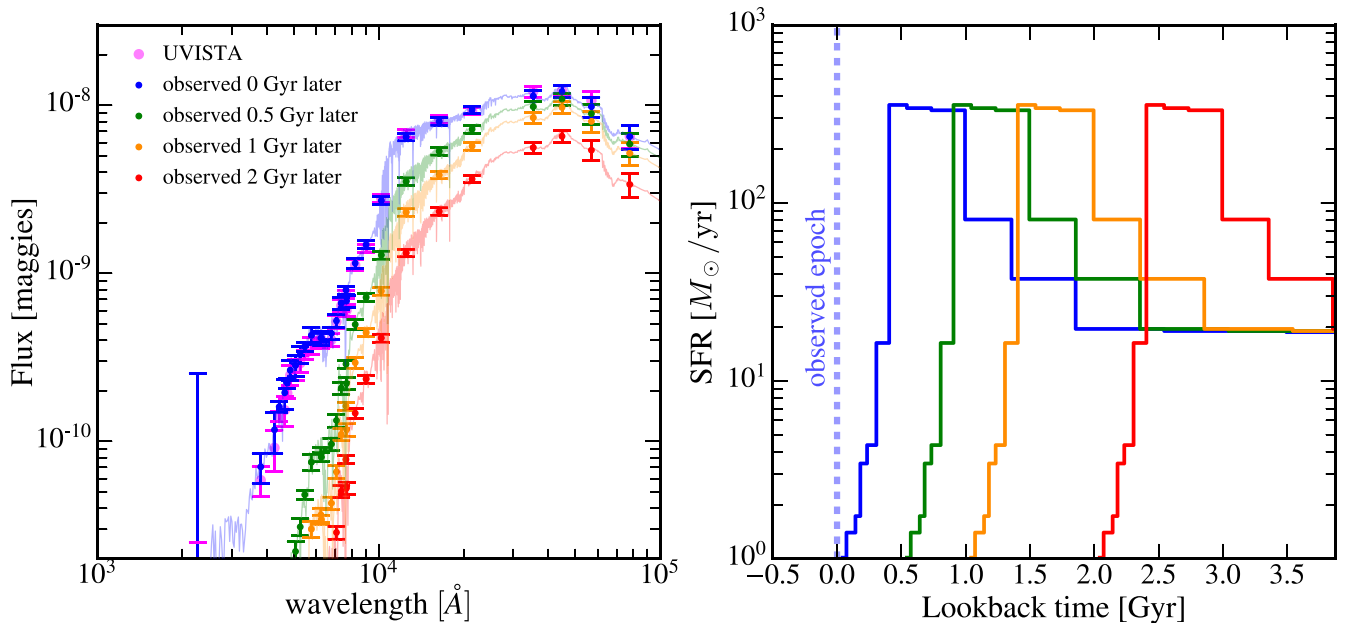


Figure A1. Left: mock photometry of UVISTA 174150 generated with MAP SFH pushed back by 0 Gyr (blue), 0.5 Gyr (green), 1 Gyr (orange), and 2 Gyr (red). Each colored line shows the mock SED generated with each SFH. We assume the same signal-to-noise ratio of the photometric measurements for each filter used in the UVISTA survey and generate mock noise, shown as error bars. The magenta points are the photometric data provided by the UVISTA catalog. Right: MAP SFH of UVISTA 174150 pushed back to account for passive evolution (the same color code used as for the left panel). The oldest bins are removed to assume the same observed epoch/redshift.

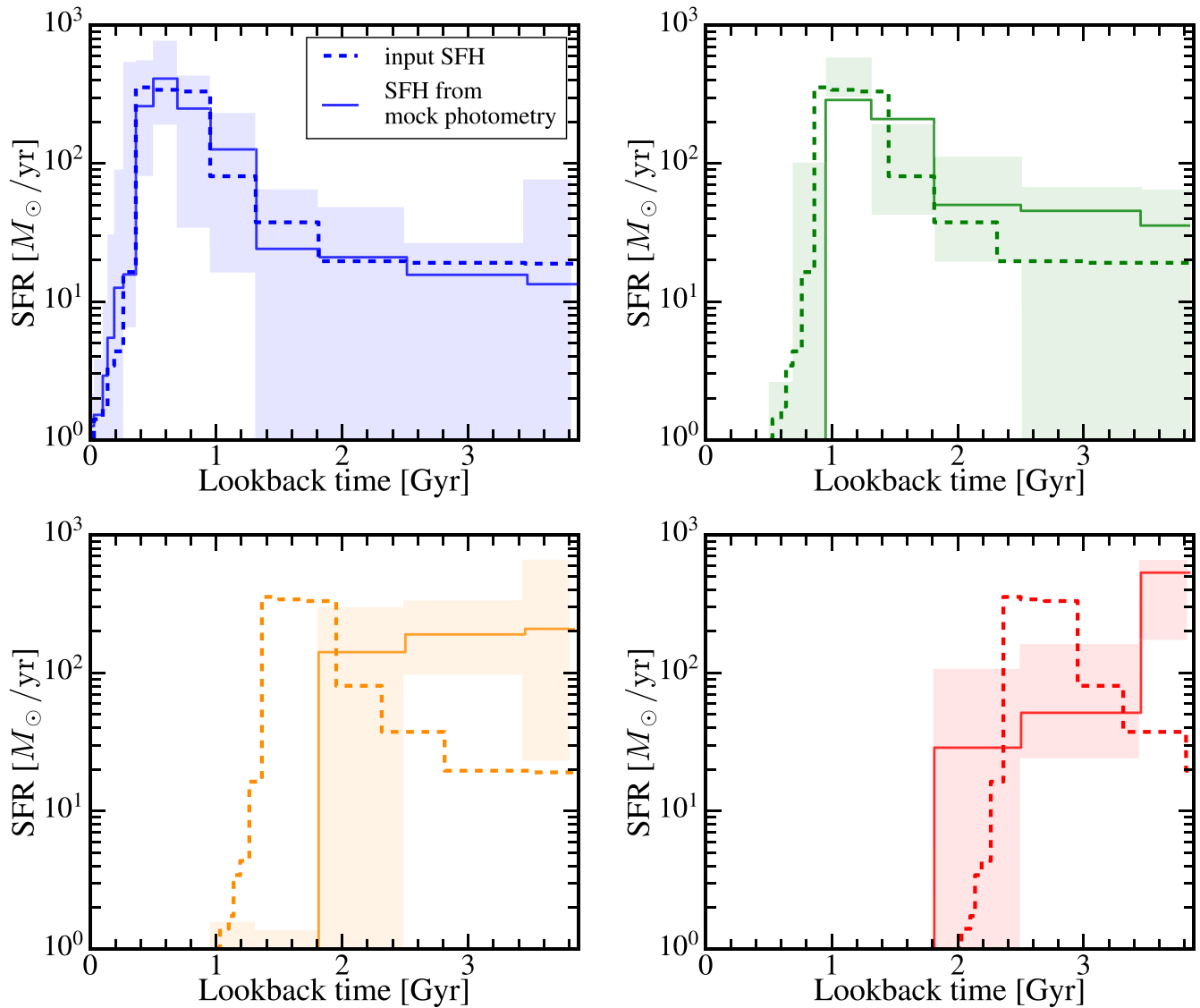





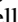





Figure A2. SFHs from the `Prospector` fitting on mock photometry generated with the SFH shifted back by 0 Gyr (blue), 0.5 Gyr (green), 1 Gyr (orange), and 2 Gyr (red). The dashed line shows the input SFH used to generated the mock photometry, and the solid line is the MAP distribution from the `Prospector` fit on the mock photometry. The shaded regions include 95% of the posterior distribution.

survey. The left panel of Figure A1 shows the mock photometric data of UVISTA 174150 when observed 0 Gyr (blue), 0.5 Gyr (green), 1 Gyr (orange), 2 Gyr (red) later. The magenta points are the photometric data provided by the UVISTA catalog. We run `Prospector` on the mock photometric data generated with shifted SFHs. Figure A2 shows the SFH from the `Prospector` fitting on the mock photometry generated with each shifted SFH. The solid line shows the MAP distribution, with shaded regions indicating 95% of the posteriors. The dashed line represents the input SFH.

The starburst and rapid quenching features do not seem to be well reproduced with `Prospector` when observed >1 Gyr after quenching. This is probably because the time (age) bins are much coarser at older ages and it is more difficult to distinguish the relative contributions of older stellar populations. Still, even observed a few Gyr later, a sharp cutoff in the SFH is reproduced by the `Prospector` fitting. Among the random ~ 100 quiescent galaxies we present in Figure 11, only \sim five to six galaxies seem to have sharp truncations in SFH a

few Gyr ago. This gives us another piece of evidence that only a small fraction of quiescent galaxies are the descendants of rapidly quenched galaxies.

ORCID iDs

Minjung Park  <https://orcid.org/0000-0002-8435-9402>
 Sirio Belli  <https://orcid.org/0000-0002-5615-6018>
 Charlie Conroy  <https://orcid.org/0000-0002-1590-8551>
 Sandro Tacchella  <https://orcid.org/0000-0002-8224-4505>
 Joel Leja  <https://orcid.org/0000-0001-6755-1315>
 Sam E. Cutler  <https://orcid.org/0000-0002-7031-2865>
 Benjamin D. Johnson  <https://orcid.org/0000-0002-9280-7594>
 Erica J. Nelson  <https://orcid.org/0000-0002-7524-374X>
 Razieh Emami  <https://orcid.org/0000-0002-2791-5011>

References

Alatalo, K., Lisenfeld, U., Lanz, L., et al. 2016, *ApJ*, 827, 106
 Almaini, O., Wild, V., Maltby, D. T., et al. 2017, *MNRAS*, 472, 1401
 Baldry, I. K., Glazebrook, K., Brinkmann, J., et al. 2004, *ApJ*, 600, 681

- Barnes, J. E., & Hernquist, L. E. 1991, *ApJL*, 370, L65
- Baron, D., Netzer, H., Poznanski, D., Prochaska, J. X., & Förster Schreiber, N. M. 2017, *MNRAS*, 470, 1687
- Barro, G., Faber, S. M., Koo, D. C., et al. 2017, *ApJ*, 840, 47
- Bekki, K., Couch, W. J., Shioya, Y., & Vazdekis, A. 2005, *MNRAS*, 359, 949
- Belfiore, F., Maiolino, R., Maraston, C., et al. 2016, *MNRAS*, 461, 3111
- Belli, S., Newman, A. B., & Ellis, R. S. 2015, *ApJ*, 799, 206
- Belli, S., Newman, A. B., & Ellis, R. S. 2019, *ApJ*, 874, 17
- Bluck, A. F. L., Mendel, J. T., Ellison, S. L., et al. 2014, *MNRAS*, 441, 599
- Brammer, G. B., van Dokkum, P. G., & Coppi, P. 2008, *ApJ*, 686, 1503
- Calzetti, D., Armus, L., Bohlin, R. G., et al. 2000, *ApJ*, 533, 682
- Carollo, C. M., Bschorr, T. J., Renzini, A., et al. 2013, *ApJ*, 773, 112
- Chabrier, G. 2003, *PASP*, 115, 763
- Charlot, S., & Fall, S. M. 2000, *ApJ*, 539, 718
- Choi, J., Dotter, A., Conroy, C., et al. 2016, *ApJ*, 823, 102
- Conroy, C., Gunn, J. E., & White, M. 2009, *ApJ*, 699, 486
- Croton, D. J., Springel, V., White, S. D. M., et al. 2006, *MNRAS*, 365, 11
- Cutler, S. E., Giavalisco, M., Ji, Z., & Cheng, Y. 2023, *ApJ*, 945, 97
- Cutler, S. E., Whitaker, K. E., Mowla, L. A., et al. 2022, *ApJ*, 925, 34
- D'Eugenio, F., van der Wel, A., Wu, P.-F., et al. 2020, *MNRAS*, 497, 389
- Davis, T. A., van de Voort, F., Rowlands, K., et al. 2019, *MNRAS*, 484, 2447
- Dekel, A., & Burkert, A. 2014, *MNRAS*, 438, 1870
- Dhiwar, S., Saha, K., Dekel, A., et al. 2023, *MNRAS*, 518, 4943
- Diemer, B., Sparre, M., Abramson, L. E., & Torrey, P. 2017, *ApJ*, 839, 26
- Diemer, B., Stevens, A. R. H., Forbes, J. C., et al. 2018, *ApJS*, 238, 33
- Dressler, A., & Gunn, J. E. 1983, *ApJ*, 270, 7
- Fagioli, M., Carollo, C. M., Renzini, A., et al. 2016, *ApJ*, 831, 173
- Fang, J. J., Faber, S. M., Koo, D. C., et al. 2018, *ApJ*, 858, 100
- Forrest, B., Marsan, Z. C., Annunziatella, M., et al. 2020, *ApJ*, 903, 47
- Förster Schreiber, N. M., Übler, H., Davies, R. L., et al. 2019, *ApJ*, 875, 21
- Franx, M., Labbé, I., Rudnick, G., et al. 2003, *ApJL*, 587, L79
- French, K. D. 2021, *PASP*, 133, 072001
- French, K. D., Yang, Y., Zabludoff, A., et al. 2015, *ApJ*, 801, 1
- Genzel, R., Förster Schreiber, N. M., Rosario, D., et al. 2014, *ApJ*, 796, 7
- Gunn, J. E., & Gott, J. R. I. 1972, *ApJ*, 176, 1
- Ji, Z., & Giavalisco, M. 2022, *ApJ*, 935, 120
- Ji, Z., & Giavalisco, M. 2023, *ApJ*, 943, 54
- Johnson, B. D., Leja, J., Conroy, C., & Speagle, J. S. 2021, *ApJS*, 254, 22
- Kennicutt, R. C. J. 1998, *ApJ*, 498, 541
- Khoperskov, S., Haywood, M., Di Matteo, P., Lehnert, M. D., & Combes, F. 2018, *A&A*, 609, A60
- Kriek, M., & Conroy, C. 2013, *ApJL*, 775, L16
- Kriek, M., van Dokkum, P. G., Franx, M., Illingworth, G. D., & Magee, D. K. 2009, *ApJL*, 705, L71
- Leja, J., Carnall, A. C., Johnson, B. D., Conroy, C., & Speagle, J. S. 2019a, *ApJ*, 876, 3
- Leja, J., Johnson, B. D., Conroy, C., et al. 2019b, *ApJ*, 877, 140
- Luo, Y., Li, Z., Kang, X., Li, Z., & Wang, P. 2020, *MNRAS Lett.*, 496, L116
- Maltby, D. T., Almaini, O., McLure, R. J., et al. 2019, *MNRAS*, 489, 1139
- Maltby, D. T., Almaini, O., Wild, V., et al. 2018, *MNRAS*, 480, 381
- Man, A., & Belli, S. 2018, *NatAs*, 2, 695
- Marinacci, F., Vogelsberger, M., Pakmor, R., et al. 2018, *MNRAS*, 480, 5113
- Martig, M., Bournaud, F., Teysier, R., & Dekel, A. 2009, *ApJ*, 707, 250
- Momcheva, I. G., van Dokkum, P. G., van der Wel, A., et al. 2017, *PASP*, 129, 015004
- Mosleh, M., Tacchella, S., Renzini, A., et al. 2017, *ApJ*, 837, 2
- Mowla, L. A., Cutler, S. E., Brammer, G. B., et al. 2022, *ApJ*, 933, 129
- Muzzin, A., Marchesini, D., Stefanon, M., et al. 2013a, *ApJS*, 206, 8
- Muzzin, A., Marchesini, D., Stefanon, M., et al. 2013b, *ApJ*, 777, 18
- Naab, T., Johansson, P. H., Ostriker, J. P., & Efstathiou, G. 2007, *ApJ*, 658, 710
- Naiman, J. P., Pillepich, A., Springel, V., et al. 2018, *MNRAS*, 477, 1206
- Nelson, D., Pillepich, A., Springel, V., et al. 2018, *MNRAS*, 475, 624
- Nelson, D., Pillepich, A., Springel, V., et al. 2019a, *MNRAS*, 490, 3234
- Nelson, D., Springel, V., Pillepich, A., et al. 2019b, *ComAC*, 6, 2
- Nelson, E. J., Tadaki, K.-i., Tacconi, L. J., et al. 2019c, *ApJ*, 870, 130
- Noiro, G., Sawicki, M., Abraham, R., et al. 2022, *MNRAS*, 512, 3566
- Park, M., Tacchella, S., Nelson, E. J., et al. 2022, *MNRAS*, 515, 213
- Pathak, D., Belli, S., & Weinberger, R. 2021, *ApJL*, 916, L23
- Peng, C. Y., Ho, L. C., Impey, C. D., & Rix, H.-W. 2002, *AJ*, 124, 266
- Pillepich, A., Nelson, D., Hernquist, L., et al. 2018, *MNRAS*, 475, 648
- Pillepich, A., Nelson, D., Truong, N., et al. 2021, *MNRAS*, 508, 4667
- Pillepich, A., Springel, V., Nelson, D., et al. 2018, *MNRAS*, 473, 4077
- Pontzen, A., Tremmel, M., Roth, N., et al. 2017, *MNRAS*, 465, 547
- Puglisi, A., Daddi, E., Liu, D., et al. 2019, *ApJL*, 877, L23
- Rodriguez-Gomez, V., Snyder, G. F., Lotz, J. M., et al. 2019, *MNRAS*, 483, 4140
- Setton, D. J., Dey, B., Khullar, G., et al. 2023, *ApJL*, 947, L31
- Setton, D. J., Verrico, M., Bezanson, R., et al. 2022, *ApJ*, 931, 51
- Silk, J., & Rees, M. J. 1998, *A&A*, 331, L1
- Snyder, G. F., Cox, T. J., Hayward, C. C., Hernquist, L., & Jonsson, P. 2011, *ApJ*, 741, 77
- Somerville, R. S., Hopkins, P. F., Cox, T. J., Robertson, B. E., & Hernquist, L. 2008, *MNRAS*, 391, 481
- Speagle, J. S. 2020, *MNRAS*, 493, 3132
- Springel, V., & Hernquist, L. 2003, *MNRAS*, 339, 312
- Springel, V., Pakmor, R., Pillepich, A., et al. 2018, *MNRAS*, 475, 676
- Strateva, I., Ivezić, Ž., Knapp, G. R., et al. 2001, *AJ*, 122, 1861
- Suess, K. A., Kriek, M., Price, S. H., & Barro, G. 2020, *ApJL*, 899, L26
- Suess, K. A., Leja, J., Johnson, B. D., et al. 2022, *ApJ*, 935, 146
- Tacchella, S., Conroy, C., Faber, S. M., et al. 2022a, *ApJ*, 926, 134
- Tacchella, S., Dekel, A., Carollo, C. M., et al. 2016a, *MNRAS*, 458, 242
- Tacchella, S., Dekel, A., Carollo, C. M., et al. 2016b, *MNRAS*, 457, 2790
- Tacchella, S., Finkelstein, S. L., Bagley, M., et al. 2022b, *ApJ*, 927, 170
- Tadaki, K.-i., Belli, S., Burkert, A., et al. 2020, *ApJ*, 901, 74
- Tadaki, K.-i., Genzel, R., Kodama, T., et al. 2017, *ApJ*, 834, 135
- Terrazas, B. A., Bell, E. F., Pillepich, A., et al. 2020, *MNRAS*, 493, 1888
- Trussler, J., Maiolino, R., Maraston, C., et al. 2020, *MNRAS*, 491, 5406
- Vacca, W. D., Cushing, M. C., & Rayner, J. T. 2003, *PASP*, 115, 389
- van der Wel, A., Bell, E. F., van den Bosch, F. C., Gallazzi, A., & Rix, H.-W. 2009, *ApJ*, 698, 1232
- van der Wel, A., Franx, M., Van Dokkum, P. G., et al. 2014, *ApJ*, 788, 28
- van Dokkum, P. G. 2005, *AJ*, 130, 2647
- Weinberger, R., Springel, V., Hernquist, L., et al. 2017, *MNRAS*, 465, 3291
- Weinberger, R., Springel, V., Pakmor, R., et al. 2018, *MNRAS*, 479, 4056
- Whitaker, K. E., Kriek, M., van Dokkum, P. G., et al. 2012a, *ApJ*, 745, 179
- Whitaker, K. E., van Dokkum, P. G., Brammer, G., & Franx, M. 2012b, *ApJL*, 754, L29
- Wild, V., Almaini, O., Dunlop, J., et al. 2016, *MNRAS*, 463, 832
- Wild, V., Heckman, T., & Charlot, S. 2010, *MNRAS*, 405, 933
- Wild, V., Taj Aldeen, L., Carnall, A., et al. 2020, *MNRAS*, 494, 529
- Wu, P.-F., van der Wel, A., Bezanson, R., et al. 2018, *ApJ*, 868, 37
- Wuyts, S., Förster Schreiber, N. M., van der Wel, A., et al. 2011, *ApJ*, 742, 96
- Yan, R., & Blanton, M. R. 2012, *ApJ*, 747, 61
- Yan, R., Newman, J. A., Faber, S. M., et al. 2006, *ApJ*, 648, 281
- Zabludoff, A. I., Zaritsky, D., Lin, H., et al. 1996, *ApJ*, 466, 104
- Zheng, Y., Wild, V., Lahén, N., et al. 2020, *MNRAS*, 498, 1259
- Zolotov, A., Dekel, A., Mandelker, N., et al. 2015, *MNRAS*, 450, 2327
- Zuckerman, L. D., Belli, S., Leja, J., & Tacchella, S. 2021, *ApJL*, 922, L32